University of Alberta

Theoretical Studies of Semiconductor Surface Modification

by

Amsalu Y. Anagaw

©

A thesis submitted to the Faculty of Graduate Studies and Research in partial fulfillment of the requirements for the degree of Master of Science

Department of Physics

Edmonton, Alberta

Spring 2007

Library and Archives Canada

Published Heritage Branch

395 Wellington Street
Ottawa ON K1A 0N4
Canada

Bibliothèque et Archives Canada

Direction du Patrimoine de l'édition

395, rue Wellington
Ottawa ON K1A 0N4
Canada

Your file Votre référence
ISBN: 978-0-494-29929-6
Our file Notre référence
ISBN: 978-0-494-29929-6

NOTICE:
The author has granted a non-exclusive license allowing Library and Archives Canada to reproduce, publish, archive, preserve, conserve, communicate to the public by telecommunication or on the Internet, loan, distribute and sell theses worldwide, for commercial or non-commercial purposes, in microform, paper, electronic and/or any other formats.

The author retains copyright ownership and moral rights in this thesis. Neither the thesis nor substantial extracts from it may be printed or otherwise reproduced without the author's permission.

AVIS:
L'auteur a accordé une licence non exclusive permettant à la Bibliothèque et Archives Canada de reproduire, publier, archiver, sauvegarder, conserver, transmettre au public par télécommunication ou par l'Internet, prêter, distribuer et vendre des thèses partout dans le monde, à des fins commerciales ou autres, sur support microforme, papier, électronique et/ou autres formats.

L'auteur conserve la propriété du droit d'auteur et des droits moraux qui protège cette thèse. Ni la thèse ni des extraits substantiels de celle-ci ne doivent être imprimés ou autrement reproduits sans son autorisation.

In compliance with the Canadian Privacy Act some supporting forms may have been removed from this thesis.

While these forms may be included in the document page count, their removal does not represent any loss of content from the thesis.

Conformément à la loi canadienne sur la protection de la vie privée, quelques formulaires secondaires ont été enlevés de cette thèse.

Bien que ces formulaires aient inclus dans la pagination, il n'y aura aucun contenu manquant.

Canada

University of Alberta

Library Release Form

Name of Author: Amsalu Y. Anagaw

Title of Thesis: Theoretical Studies of Semiconductor Surface Modification

Degree: Master of Science

Year this Degree Granted: 2007

Permission is hereby granted to the University of Alberta Library to reproduce single copies of this thesis and to lend or sell such copies for private, scholarly or scientific research purposes only.

The author reserves all other publication and other rights in association with the copyright in the thesis, and except as herein before provided, neither the thesis nor any substantial portion thereof may be printed or otherwise reproduced in any material form whatsoever without the author's prior written permission.

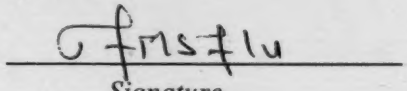

Signature

Jan. 22, 2007

To My Parents and Alebachew Embiale

Abstract

The electrical properties of silicon can be fine-tuned by covalent attachment of para-substituted styrene molecules. In the first part of this thesis, pathways for the radical mediated self-directed growth of styrene molecular lines on H-Si(100)-2x1 and H-Si(100)-3x1 were studied theoretically. In the second part of the thesis, the change in the electronic properties of H-Si(100)-2x1 with different coverage of para-substituted styrene molecules, with various electron-withdrawing and donating groups, was studied. The work function change was found to correlate linearly with surface dipole moment of the molecular layer. A direct quantitative correlation between the isolated dipole moments with the work function was also observed. Despite large differences in the dipole moments of the isolated molecules, the interface dipole moment between the molecular layer and the silicon surface, which results from charge transfer across the interface due to bond formation, is found to be fairly constant with molecule type.

Acknowledgments

I would like to express my heartfelt thanks to my supervisors, Prof. Robert A. Wolkow and Dr. Gino A. DiLabio for giving me the opportunity to study my MSc in the MSD group and whose enthusiasm and expertise were greatly appreciated. Without their assistance and support, this research would not have been possible. I have benefited from numerous people and many facilities during my graduate study in the MSG group. There is no point to complain about, this is the type of team work I would like to have throughout my career.

My hearty thanks to my excellent supervisor Gino for making this thesis possible, for assistance in key issues, for enlightening discussions and for his advice and encouragement through the last two years. He has been a source of valuable advice and has always been on hand to respond positively to the query. My work would be impossible without the permanent interest and advice of Gino.

Finally, I would also like to thank the committee members. I thank all friendly people around me for the good atmosphere and permanent support. I would special thank my mom W/o Adna Alebachew, my father and my sisters.

Table of Contents

List of Tables

List of Figures

Abstract

CHAPTER 1 Introduction 1

1.1. Properties of the silicon substrate 2
1.2. Adsorption of Organic molecular layers 5
1.3. Self-directed growth of Styrene lines 6
1.4. Surface modification 8
1.5. Summary of thesis work 9

CHAPTER 2 Theory 11

2.1. Many-Body Problem 11
2.2. Born-Oppenheimer Approximation 13
2.3. Hartree-Fock theory 13
2.4. Exchange and correlation 15
2.5. Density Functional Theory (DFT) 15
2.6. Basis sets and Pseudopotentials 21

CHAPTER 3 Computational methods 23

3.1. Self-directed growth of one-dimensional (1D) styrene lines 24
3.2. Surface Work function Calculations 25
3.2.1. Modeling the structure 26

CHAPTER 4 Result and discussion 31

4.1. Self directed growth of styrene molecules 31
4.1.1. Growth on H-Si(100)-2x1 surface 31

4.1.2. Growth on H-Si(100)-3x1 surface 35
4.2. Work function changes with 4-X-Styrene molecular functionalization of H-Si(100)-2x1 40
4.2.1. Full monolayer coverage (X= OCH_3 , CH_3 , H, COOH, CF_3) 43
4.2.2.1. Clean and hydrogen terminated Si(100)-2x1 surfaces 43
4.2.2.2. Change in work function of the H-Si(100)-2x1 surface with 4-X-Styrene adsorption 47
4.2.2.3. Deconvoluting the Surface Dipole by examining the molecular and chemisorption contribution to $\Delta\Phi$ 49
4.2.2.4. Charge transfer at the interface between organic molecular layer and Si surface 59
4.2.2. Half monolayer coverage(X= $N(CH_3)_2$, NH_2 , OCH_3 , CH_3 , H, COOH, CF_3, OC_2F_3, CN , NO_2) 63

CHAPTER 5 Conclusions 68

Bibliography 70

Appendix A. Vienna Ab initio Simulation Package (VASP) 75

A.1. K-point Sampling 80

Appendix B. Testing the simulation parameters 83

B.1. K-point convergence 83
B.2. Cutoff energy convergence 86

Appendix C. FLOWCHART 91

C.1. Flowchart showing 92

List of Tables

Table 4.1 Calculated barrier heights, $E_{bar,}$ and reaction energies, ΔE, for the processes shown in Fig. 4.1. 34

Table 4.2 Calculated barrier heights, $E_{bar,}$ and reaction energies, ΔE, for the processes shown in Fig. 4.2. 36

Table 4.3 Step in vacuum electrostatic potential ΔV_{ML} across the molecular layer, left and right ionization potentials (IP_{left} and IP_{right}) of the layers of molecules and molecular dipole (μ_{ML}) of the layers at full coverage for 4-X-syrene. X denotes the substituents 55

Table 4.4 Change in the work function ($\Delta\Phi$(eV)) of an H-Si(100)-2x1 upon the adsorption of 4-X-syrene, surface dipole (μ_z), molecular dipole (μ_{ML}) and the chemisorption dipole moment (μ_{chem}) and Fermi energy (E_F) at full monolayer coverage. Dipole moments are in Debye. 56

Table 4.5 Change in the work function ($\Delta\Phi$(eV)) of an H-Si(100)-2x1 upon the adsorption of 4-X-syrene, surface dipole (μ_z), molecular dipole (μ_{ML}), the chemisorption dipole moment (μ_{chem}) and the Fermi energy (E_F) at half monolayer coverage. Dipole moments are in Debye. 64

Table B.1 Energy change per atom calculated at different k-point meshes and irreducible k-points. 85

Table B.2 Convergence of cohesive energy change per atom calculated at different cutoff energies. 86

List of Figures

Figure 1.1 Unit cell for the face centered cubic diamond lattice structure of silicon. Lattice directions are indicated in square brackets. 2

Figure 1.2 Silicon (100) reconstructed surfaces. (a) Hydrogen terminated Si(100)-2x1 surface and (b) Hydrogen terminated Si(100)-3x1 surface. 4

Figure 1.3 A simple representation of styrene molecule (a) and molecular structure of styrene (b). 7

Figure 1.4 A simple schematic representation for styrene self-directed growth on H-Si(100)-2x1 surface. (a) Styrene molecule and a radical H-Si(100)-2x1 surface. (b) Styrene molecule adsorption on an H-empty site. (c) Final state after hydrogen atom abstraction from the next dimer. 7

Figure 3.1 The para-substituted styrene (4-X-styrene) molecules considered in the simulations. 26

Figure 3.2 Adsorption of styrene molecule on H-Si(100)-2x1 surface (a) unit cell used for 1 ML calculations on a 2x1 unit cell and -NO_2 functional group attached (b) on 4x1 unit cell, 0.5 ML converge. 28

Figure 3.3 Top view of adsorption of styrene molecule on H-Si(100)-2x1 with adsorbed styrene molecules at 1 ML (a) and at 0.5 ML (b) coverage. The 2x1 and 4x1 surface unit cells are indicated by rectangles. 30

Figure 4.1 Possible reaction pathways for styrene self-directed growth on H-Si(100)-2x1 surface. (A) Styrene molecule approaches a 2x1 surface with a preexisting dangling bond on a dimer row. (B) Styrene molecule adsorption on

H-Si(100)-2x1. (C) Transition state for hydrogen abstraction from the same dimer. (D) Final product after hydrogen abstraction from the same dimer. (E) Transition state for hydrogen abstraction from the next dimer. (F) Final product after hydrogen abstraction from the next dimer. 32

Figure 4. 2 Possible reaction pathways for styrene self-directed growth on the H-Si(100)-3x1 surface. (A) Styrene molecule approaches a 3x1 surface with a preexisting dangling bond on a dimer row. (B) Styrene molecule adsorption on an H-empty site. (C) Hydrogen abstraction from the monomer row. (D) Hydrogen abstraction from the same dimer. (E) Hydrogen abstraction from the next dimer along the row. (F) Final product after hydrogen abstraction from the adjacent monomer site. (G) Final product after hydrogen abstraction from the same dimer. (H) Final product after hydrogen abstraction from the next dimer. 38

Figure 4.3 The proposed mechanism of styrene chain reaction on H-Si(100)-3x1 surface in the cross-row direction. (a) Final state after abstraction of an H atom from the adjacent monomer. (b) Inversion of H atom on the monomer site. 39

Figure 4.4 Schematic representation of (a) the buckled dimer in the Si(100)-2x1 surface and (b) dimer in the hydrogen terminated Si(100)-2x1 surface. 43

Figure 4.5 A 2x2 surface unit cell of the (a) Si(100)-2x1 surface and (b) H-Si(100)-2x 1 surface used in the calculations. 44

Figure 4.6 An averaged relative planar electrostatic potential of a clean Si(100-2x1 and H-Si(100) surface as a function of position [100] direction. The Fermi energy is set to zero, V-E_F. The inset shows a "Ball and Stick" representation of the surface. The vertical lines correlate the position of the bottom and the top silicon atomic layers with the electrostatic potential. 45

Figure 4.7 Planar averaged electrostatic potential for 1 ML coverage of different aromatic molecules adsorbed on H-Si(100)-2x1 as a function of position, in the direction perpendicular to the surface. The left side represents the work function of H-Si(100)-2x1 and the right side represents the modified work function of the surface upon the adsorption of 4-X-styrene molecules, written on the plot. The Fermi level is set to zero. The inset shows a "Ball and Stick" representation of the silicon atomic layers and molecules. The vertical lines show the position of the bottom and the top silicon atomic layers. X denotes where the substituents are placed. 48

Figure 4.8 Schematic representations of modification of a silicon surface with an organic molecular layer. (a) Molecular layer on a surface. (b) A molecular monolayer is formed in the same geometry as it was in (a). (c) An H-Si(100)-2x1 surface with half H monolayer coverage. Arrows indicate the direction of the surface dipole moment, molecular and interface dipole moments. For example for EDGs, charge density per unit area created in the monolayer is indicated, σ^+ and σ^-. X denotes where the substituents are placed. 51

Figure 4.9 Plane averaged electrostatic potential of styrene and para-substituted styrene molecular layers perpendicular to the surface as a function of the position inside the unit cell. The inset shows a "Ball and Stick" representation of the molecule. 54

Figure 4. 10 Conjugation between π-type molecular orbital of the functional groups (a) NO_2 and (b) OCH_3 with the ring. 57

Figure 4.11 Change in work function with molecular dipole moment ($\sigma = 0.89$ and $R^2 = 1.00$) and free molecule net dipole moment ($\sigma = 1.92$ and $R^2 = 0.94$) at full ML coverage. Substituents are indicted. 58

Figure 4.12 Planar averaged electron density differences for CF_3-Styrene (blue) and styrene (red) ML on an H-Si(100)-2x1 surface. Both are the functions of z, the direction perpendicular to the surface. The inset shows a "Ball and Stick" representation of the silicon atomic layers and molecules. The vertical lines show the position of the top Si and the bottom C atoms. 61

Figure 4.13 Change in work function with molecular dipole moment (σ = 1.03 and R^2 =1.00) and free molecule net dipole moment (σ = 3.33 and R^2 =0.98) at 0.5 ML coverage. 66

Figure B.1 The diamond structure of silicon (a) and its primitive cell (b) 83

Figure B.2 Convergence of Si cohesive energy versus number of k-points per direction. 84

Figure B.5 (a) Band structure of silicon along a high symmetry line obtained by GGA-PBE functional at the equilibrium lattice constant. (b) The DOS of silicon bulk crystal. 90

CHAPTER 1

Introduction

The modification of semiconductor surfaces by the attachment of various unsaturated organic molecules has potential applications in semiconductor technology in fields such as molecular electronics, chemical and biological sensor devices and so on [1-5]. The ability to control the growth of nanoscale organic structures and the electronic properties on a semiconductor surface has also enormous potential for realizing a variety of novel hybrid organic semiconductor applications. The properties of semiconductor surfaces can vary over wide range upon adsorption of covalently bound organic molecules. Control over the electronic properties of surfaces is required if constructs of these types are to be used as electronic devices.

The properties of silicon in general make it a promising semiconductor substrate for molecular electronic components for future technologies because silicon is: compatible with organic molecules, the basic material for existing microelectronics, and can be manufactured to create very different structures [5-9]. Because of its widespread use in microelectronic devices, Si(100) is chosen as the substrate for all studies in the present work. The Si(100) provides an ideal platform for building hybrid devices by seeding unsaturated hydrocarbons on templates formed from the directional dangling bonds of the (100) surface. The Si(100) the surface reconstruction gives rise to the formation of Si-Si dimers which react with molecules containing a double C=C bond. These adsorb with relatively low energy barriers, giving rise to stable covered surfaces. In addition to C, Si can also form strong covalent bonds with other elements commonly present in organic molecules, including N, O and H.

Among a number of methods for preparing films of organic molecules on different semiconductors, a particularly promising approach to form an organic layer on

silicon surface is through the use of a surface chain reaction of terminally unsaturated organic molecules on incomplete hydrogen-terminated Si surfaces. For example, the reaction mechanism of alkene molecules with H-Si(100) has been shown to lead to the formation of linear nanostructure of molecules attached to the surface through C-Si bonds [10-14].

This chapter will begin with an overview of the structure of the clean and reconstructed Si(100) semiconductor surface, as the structure and properties of these surfaces are crucial for understanding their reactivity with organic molecules. This overview is followed by a summary of the previous work investigating the reactivity of organic molecules on the Si(100) surface and the control over the electronic properties of the semiconductor surface. Finally, the major goal of this thesis is presented.

1.1. Properties of the silicon substrate

Silicon crystals have a face centered cubic diamond lattice structure in which the atoms are sp^3 hybridized to form a tetrahedral bonding configuration as shown in Fig. 1.1.

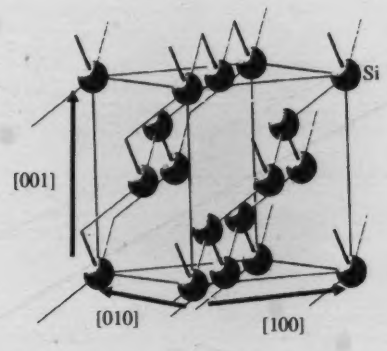

Figure 1.1 Unit cell for the face centered cubic diamond lattice structure of silicon. Lattice directions are indicated in square brackets.

It is possible to obtain a Si(100) surface reconstruction by cutting a bulk Si crystal. The cutting results in the formation of two dangling bonds per surface atoms. In order to minimize the surface energy, the surface atoms reorganize the bonding among themselves to reduce the number of the dangling bonds, a process known as surface reconstruction. The reconstruction of the Si(100)-2x1 surface structure consists of Si dimer rows with periodicity of 1 unit along the dimer row and 2 units perpendicular to the row. Although the numbers of dangling bonds are reduced by the reconstruction, the surface is still highly reactive.

The Si(100)-2x1 reconstructed surface mimics an alkene organic reagent because the two bonds of a surface Si dimer can be considered as double bonds consisting of a σ-bond and a π-bond. The π-bond in a Si dimer is sufficiently weak that the dimer is actually not held in a symmetric configuration. The strength of the π-bond interaction is estimated to be approximately 0 22-0.43 eV [15, 16]. The weak dimer π-bond plays a critical role in the reactivity of the clean Si(100)-2x1 surface. Reactions between clean silicon dimers and conjugated organic molecules (C-C π-bond), for example alkenes [17], tend to occur with little or no activation barrier.

Under suitable preparation conditions, oxide-free, hydrogen-terminated silicon surfaces can be obtained by the adsorption of atomic hydrogen under ultra-high vacuum conditions. Depending on the exposure to hydrogen atom, the surface undergoes several reconstruction patterns that can be all understood in terms of different arrangements of symmetric silicon dimers. Of the possible rearrangements of the surface following the exposure of hydrogen atom, two reconstructions are H-Si(100)-2x1 and H-Si(100)-3x1 [18].

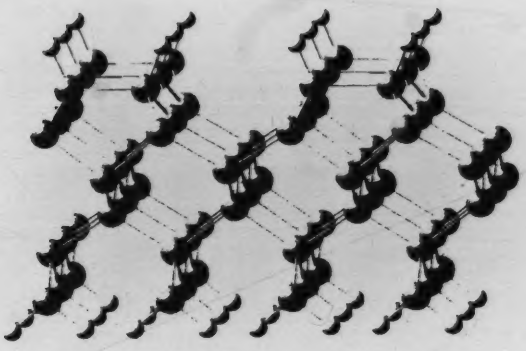

(a)

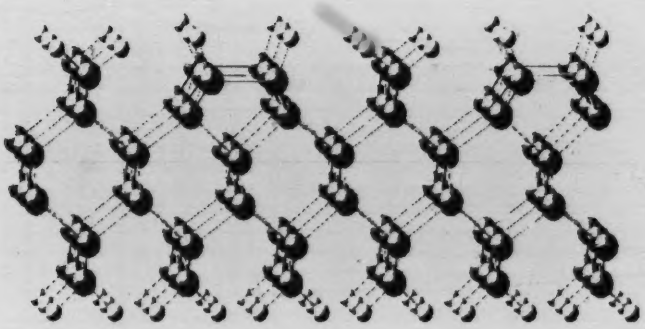

(b)

Figure 1.2 Silicon (100) reconstructed surfaces. (a) Hydrogen terminated Si(100)-2x1 surface and (b) Hydrogen terminated Si(100)-3x1 surface.

Fig. 1.2 a and b show the hydrogen terminated Si(100)-2x1 and 3x1 surfaces, respectively. In the H-Si(001)-2x1 monohydride structure, all dimer silicon-dangling bonds are capped by a hydrogen atom. The dimers become symmetric. On the H-Si(001)-3x1 surface, all silicon dangling bonds are also saturated, but it has alternating dimer rows and dihydride SiH_2 monomers.

1.2. Adsorption of Organic molecular layers

In the late 1980s, the reactions of several simple alkenes, including ethylene, propylene, and acetylene, with the Si(100) surface were investigated. At room temperature, alkenes chemisorb onto the surface in contrast to saturated organic molecules such as methane and propane, which display no reaction. Organic functionalization of Si(100) surface [5] using alkenes, occur via cycloaddition. Cycloadditions are reactions in which two molecules with π bonds come together to form a new cyclic molecule by breaking the π-bonds and creating two new σ bonds. Due to the analogy between the Si–Si dimer on the Si(100)-2x1 surface and the C=C π-bond in an alkene, certain parallels might be expected to exist between reactions between alkenes and those involving alkenes and the silicon surface [5].

Most organic materials used in experimental organic electronic devices are conjugated molecules. Conjugate molecules such as aromatic hydrocarbons like benzene and chain-like alkenes are used. Conjugated molecules possess π-electrons, which are delocalized over more than two carbon atoms within the molecule. The delocalized π-electrons between neighboring molecules determine the electron transport properties of the molecular solids in these conjugated molecules and are present in most conducting polymer materials [19]. On the other hand, unlike chain-like alkenes, aromatic hydrocarbons are more stable due to their ring structure. The cycloaddition reactions are also applicable to adsorption of aromatic hydrocarbons. For example, cycloaddition of the styrene occurs through the reaction of the vinyl group with a bare dimer on the Si(100)-2x1 surface.

Organic functionalization of semiconductors surface is a promising growth area in the development of new semiconductor-based materials and devices. It exploits the properties of organic and inorganic materials, and may lead to molecular recognition and chemical or biological sensing applications. As the range of applications for semiconductor materials continues to expand, methods that can be used to tailor their surface properties become increasingly important.

Organic modification is one means of providing new functionality to the semiconductor surface by depositing layers of organic molecules at the surface using either wet chemistry or vacuum based (dry) methods. The organic molecules can be physisorbed (by van der Waals interactions) or chemisorbed (chemical reaction with the surface). Organic molecular monolayers can also be deposited on germanium (Ge) [20]. The incorporation of organic materials at the surface offers a flexible way to tune to the properties of the surface through chemisorption of self-assembled organic ML molecules on a surface. This is a potentially powerful and flexible approach to fine-tuning the desired electronic properties of the surface and interface to yield hybrid and multifunctional systems.

1.3. Self-directed growth of Styrene lines

A unique technique for the fabrication of order arrays of organic molecules on hydrogen terminated silicon surface [5, 21] is the so-called self-directed growth mechanism. This process allows for the rapid parallel production of hybrid organic-silicon nanostructures. The formation of molecular nanostructures using the self-directed growth mechanism uses a chemical chain reaction to grow linear structures from initiated Si radical reactive sites. Nanopatterns of organic molecules, for example styrene, can be obtained on the Si surface via Si-radical formation with a STM. The chain reactions of styrene starts from a Si radical site [11]. A styrene molecule has one π bond in the vinyl group between the two carbon atoms and three π-bonds, which are delocalized around the phenyl ring (see Fig. 1.3).

(a) (b)

Figure 1.3 A simple representation of styrene molecule (a) and molecular structure of styrene (b).

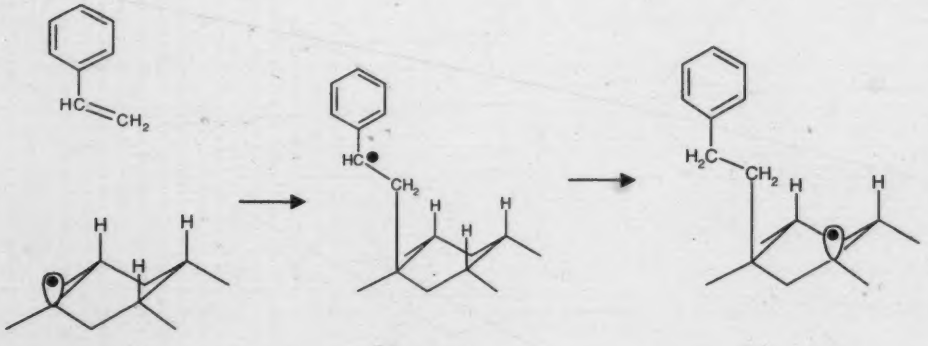

(a) (b) (c)

Figure 1.4 A simple schematic representation for styrene self-directed growth on H-Si(100)-2x1 surface. (a) Styrene molecule and a radical H-Si(100)-2x1 surface. (b) Styrene molecule adsorption on an H-empty site. (c) Final state after hydrogen atom abstraction from the next dimer.

The self-directed growth mechanism of styrene molecule on an H-passivated Si(100) surface is as follows. A styrene molecule reacts via its vinyl group to a

single silicon-dangling bond, which is generated by the removal of a hydrogen atom using the tip of the scanning probe microscope (STM) or by incomplete H-termination. The reaction involves the interaction of C-C π bond with the unpaired dangling bond on the silicon. As a result, the π bond in the vinyl group breaks to form one C-Si σ-bond and creates a carbon-centered radical (see Fig. 1.4b). Subsequently, the carbon centered radical produced in the intermediate state could be stabilized by abstracting a hydrogen atom from the nearest neighboring silicon dimer, creating a new radical (hydrogen empty site) on the next dimer in the same row (Fig. 1.4c). This new surface Si radical is ready to accept another molecule. The process can continue, leading to a chain reaction that grows a one-dimensional molecular line along the dimer row. Because of the stability of the physisorbed molecule on a surface, not all unsaturated molecules containing C=C double bond undergo chain reaction. For example alkenes smaller than 1-heptene do not grow lines, while larger alkenes up to 14 C atoms (for instance 1-undecene) long do grow lines on H-Si(100) [22].

1.4. Surface modification

Upon covalently binding an organic molecule on the semiconductor surface, the electronic properties of the surface such as the work function, electron affinity, ionization energy, band bending, interface and surface dipole moment, molecular alignment around the conduction and the valance band can be modified substantially [23]. Adsorption of molecules on a surface, by both chemisorption and weak interaction (physisorption) can alter the surface dipole considerably [24, 25]. The change in the surface dipole in turn changes the electronic properties of the surface. Adsorbing different organic molecules, for instance, thiols [26], benzoic acid derivatives [27], dicarboxylic acids [28], causes certain surface electronic properties to be varied. This occurs because different molecules have different dipole moments and frontier orbitals energies (highest occupied molecular orbital (HOMO) and lowest unoccupied molecular orbital (LUMO)). The different dipole moments of the adsorbates and their reactivities on the surface change its electronic properties.

Hill et al [29] studied the molecular level alignment at organic semiconductor/metal interfaces and found that interface dipoles are present at all of the organic layer/metal interfaces. Their work showed that interface dipoles cause the formation of dipole barriers, which play an important role for electronic transport and injection of charge carriers into organic layers. They also showed that for metals, the surface dipole between organic layers and metal depends on factors like the metal work function and the electron affinity of the organic layer. In addition, the dipole moment of the deposited organic molecules has a strong influence on the electronic structure of the semiconductor. For example, the work function of GaAs depends on the dipole moment of benzoic acids on n-GaAs [30]. Moreover, Park et al [31] showed a linear dependence between the interface dipole and the electron affinity of differently treated n-GaAs(100) surfaces onto which PTCDA was deposited. Interface dipoles occur between materials with very different ionization energies and electron affinities, for example between the high electron affinity molecule PTCDA and the lower ionization energy molecule Alq3 [32].

1.5. Summary of thesis work

This thesis focuses on the understanding of the details of the self-directed line growth process (Section 4.1) and the changes to the electronic properties of the Si surface that accompany surface modification.

To gain further understanding of the self-directed growth mechanism of styrene molecular lines on H-passivated Si(100)-2x1 and 3x1 surfaces, the processes are investigated using quantum mechanical calculations in a periodic system with the PBE functional in Chapter 4 Section 4.1. Several abstraction pathways on an H-passivated Si(100) surface have been studied.

To understand how the line growth process might be used in order to modify the electric properties of a Si surface, a variety of organic molecules has been considered. The modification of the electronic properties of silicon surface using covalently attached organic monolayers on silicon surface has been discussed in

Chapter 4 Section 4.2. This work focuses on the change in the surface work function of Si(100)-2x1 following the adsorption of different styrene derivatives. The analysis focuses on the dipole-related phenomena to the shift in the work functions. Para-substituted styrenes with different functional groups on the benzyl ring, possessing a wide range of dipole moments, are used to form a molecular layer. The changes in electronic properties (i.e. charge transfer, dipole moment, and ionization energy) of the organic layers or of the interface between the organic layer and a silicon surface as a function of the chemical substituents are investigated. This offers the opportunity to engineer some properties of silicon using organic molecules.

CHAPTER 2

Theory

In this chapter, *ab initio* approaches for finding the electronic structure of solids through the Schrödinger equation are described. The *ab initio* calculations in this thesis are performed using the Vienna Ab initio Simulation Package (VASP) [33-36]. VASP performs *ab initio* quantum mechanical calculations and molecular dynamics simulations using pseudopotential and plane wave basis sets. Various approaches for solving the time independent Schrödinger many body Schrödinger equation are discussed in this chapter, starting with the Born-Oppenheimer and Hartree approximations. The exchange-correlations of electrons are then discussed within the context of the single electron equations. The development of density functional theory and the plane wave method as a basis functions are also discussed (see Appendix)

2.1. Many-Body Problem

Ab initio electronic structure methods, which use quantum mechanics to calculate the electronic properties of a system by solving the Schrödinger equation, can be used to determine the electronic properties of a system. This is done by finding solutions of the time independent Schrödinger equation

$$\hat{H}\Psi(\vec{x},\vec{R}) = E\Psi(\vec{x},\vec{R}) \qquad (2.1)$$

where $\vec{x} = (\vec{r},\vec{s})$, and $\Psi(\vec{x},\vec{R}) = \vec{\Psi}(\vec{s}_1, \vec{s}_1, \ldots; \vec{r}_1, \vec{r}_1, \ldots; \vec{R}_1, \vec{R}_2, \ldots)$ is the many-particle wave function.

For a system composed of N_e electrons at coordinates $\vec{r}_1, \vec{r}_1, \ldots \vec{r}_{N_e}$ and N_n nuclei (charges $Z_1, Z_2, \ldots, Z_{N_n}$) at coordinates $\vec{R}_1, \vec{R}_2, \ldots \vec{R}_{N_n}$, the many-particle non-relativistic Hamiltonian can be written as follows

$$\hat{H} = \hat{T}_N + \hat{T}_e + \hat{V}_{ee}(\vec{r}) + \hat{V}_{NN}(\vec{R}) + \hat{V}_{Ne}(\vec{r},\vec{R}) \tag{2.2}$$

Using atomic units where $\frac{e^2}{4\pi\varepsilon_o} = 1$, these individual terms are written as

$$\hat{H} = \sum_{I=1}^{N} \frac{\vec{P}_I^2}{2M_I} + \sum_{i=1}^{N_e} \frac{\vec{p}_i^2}{2m_e} + \sum_{i>j} \frac{e^2}{|\vec{r}_i - \vec{r}_j|} + \sum_{I>J} \frac{Z_I Z_J e^2}{|\vec{R}_I - \vec{R}_J|} - \sum_{I,i} \frac{Z_I e^2}{|\vec{R}_I - \vec{r}_i|} \tag{2.3}$$

Eq. 2.1 therefore becomes

$$[\hat{T}_N + \hat{T}_e + \hat{V}_{ee}(\vec{r}) + \hat{V}_{NN}(\vec{R}) + \hat{V}_{Ne}(\vec{r},\vec{R})]\Psi(\vec{x},\vec{R}) = E\Psi(\vec{x},\vec{R}) \tag{2.4}$$

where $\hat{T}_N$ is the kinetic energy of the nuclei (of mass M_I), $\hat{T}_e$ is the kinetic energy of the electrons (of mass m_e), $\hat{V}_{ee}(\vec{r})$ is the electron-electron interaction, $\hat{V}_{NN}(\vec{R})$ is the nuclear-nuclear interaction and $\hat{V}_{Ne}(\vec{r},\vec{R})$ is the electrostatic interaction between the electron and the nuclei.

The wave function is a function of all electronic and nuclear coordinates. This Hamiltonian is a zeroth order expression, which describes a particular system. It omits other effects such as spin-orbit coupling, magnetic effects, and mass-velocity effects, and all resulting from relativistic corrections. However, these corrections can be handled within perturbation theory provided that the zero order wave function can be obtained. Relativistic effects are not important in the present work.

It is not possible to solve Eq. 2.4, exactly for more than one electron and it is certainly impossible to solve it exactly for a large periodic system. Therefore, it is essential to make certain well-defined approximations with the aim of reformulating the problem to make it computationally solvable. For this reason, we use approximations that render the Schrödinger equation tractable to numerical solution, whilst retaining as much as the physics of the system. The following sections describe approximate solutions to the Schrödinger equation.

2.2. Born-Oppenheimer Approximation

The essence of the Born-Oppenheimer Approximation [37] (also known as Adiabatic Approximation) is that the nuclei, being so much heavier than electrons, move relatively slowly in comparison with electrons and may be treated as stationary while the electrons move relative to them. Thus, the electron distribution of a system is primarily dependent on the position but not the velocity of the nuclei, which allows the nuclear and electronic motion of the system to be separated and solved independently. This sets the kinetic energy of the nuclei to zero and the nuclear-nuclear interaction term becomes a constant and so can be made zero or it can be added at the later time.

The Born-Oppenheimer Approximation makes it possible to solve the Schrödinger equation for only the electronic wave function of a system. Nonetheless, the electron energy depends on the nucleus positions (electrons adiabatically follow the nuclei)

$$\Psi(\vec{x};\vec{R}) \approx \underbrace{\psi(\vec{R})}_{nuclei} \cdot \underbrace{\psi(\vec{x};\vec{R})}_{electrons} \qquad (2.5)$$

The electronic structure of a system can be obtained by solving the Schrödinger Equation with the simpler Hamiltonian given by

$$\hat{H}_e \Psi(\vec{x}) = [\hat{T}_e + \hat{V}_{ee}(\vec{r}) + \hat{V}_{Ne}(\vec{r},\vec{R})]\Psi(\vec{x}) = E_e(\vec{R})\Psi(\vec{x}) \qquad (2.6)$$

Note that, the Born-Oppenheimer approximation sometimes does not work when the correlations between ionic and electronic motion are important. Despite the simplification, Eq. 2.6 is not still easy to solve and approximation methods are required. These are discussed in the following sections.

2.3. Hartree-Fock theory

The Hartree-Fock (HF)[38] method is based on the assumption that every electron moves in the potential created by the nuclei plus the average potential of all the

other electrons. It is an independent-particle model in which electron correlation is neglected. A many particle wave function describing electrons is forced to obey the Pauli principle, i.e., no electrons in the same system are allowed to have the same set of quantum numbers; to be precise the wave function needs to be antisymmetric. One such wave function is represented by the Slater or Slater-Fock determinant. In the Slater determinant, exchanging the coordinates of two electrons is the same as the exchanging two rows, with a resulting a change in sign which keeps the antisymmetry of the wave function. An example of Slater determinant for N electrons system is

$$\Psi(\vec{r}_1,.....\vec{r}_N)=\frac{1}{\sqrt{N!}}\begin{vmatrix}\Psi_1(\vec{r}_1) & \Psi_1(\vec{r}_2) & \cdots & \Psi_1(\vec{r}_N)\\ \Psi_2(\vec{r}_1) & \Psi_2(\vec{r}_2) & \cdots & \Psi_2(\vec{r}_N)\\ \vdots & \vdots & & \vdots \\ \Psi_n(\vec{r}_1) & \Psi_N(\vec{r}_2) & \cdots & \Psi_N(\vec{r}_N)\end{vmatrix} \qquad (2.7)$$

For the sake of simplicity, the spin coordinates of the wave functions are not written explicitly but should be included in each spatial wave function. The expression in Eq. 2.7 describes N electrons occupying N spin orbitals $(\Psi_1,\Psi_2,\cdots,\Psi_N)$. A spin orbital is a product of a spatial orbital and one of the two orthonormal functions α and β describing spin up and spin down, respectively. The factor $1/\sqrt{N!}$ is normalization constant and Ψ_i indicates both spatial and spin coordinates.

By varying the spatial part of the Slater determinant, i.e., the molecular orbitals, the total energy can be minimized. The solution is an approximation because the Coulomb interaction between electrons is approximated by a self-consistent field. Thus, the exact solution cannot be a product of one-particle wave functions. Since $|\Psi|^2$ must be invariant to the exchange of space and spin coordinates of any two electrons, Eq. 2.7, introduces exchange effects. This means the correlated motion of two electrons with the same spin are included. However, the correlated motion

between electrons with different spins is not included. For this reason, the Hartee–Fock approximation fails to describe the correlated motion of electrons.

The main idea behind the Hartee–Fock Equation is that the many-body problem is approximated by a self-consistent calculation of the energy of one electron in the average potential generated by the rest of the electrons.

2.4. Exchange and correlation

According to the Pauli principle, the wave function of a many-electron system must be antisymmteric under the exchange of any two electrons. This in turn reduces the Coulomb energy of the electronic system because there are larger spatial separations between electrons that have the same spin. The reduction in the energy of the electronic system due to the antisymmetry of the wave function is called the exchange energy. This energy is included in the Hartree-fock approximation. The Coulomb energy of the electronic system can be further reduced below its value when electrons that have opposite spins are also spatially separated. The correlation energy is simply the difference in energy between the full correlation energy and the Hartree-Fock energy obtained by including only the exchange due to the Pauli principle. It results from the fact that the motion of the individual electrons is not independent but rather they repel each other due to Coulomb repulsion. This is the most difficult part of electronic structure simulations in terms of computational effort.

2.5. Density Functional Theory (DFT)

In the Hartree–Fock approximation, the Slater determinant is introduced and used to determine the wave functions for the system. Knowing the wave functions, it is possible to determine the property of interest. However, solving many dimensional wave function is time consuming and often impractical. Another approach is Density Functional Theory (DFT), which considers the electron density rather than the many-body wave function as a central variable. This approach reduces the difficulty of the problem substantially. The density is a function of three variables,

i.e., it only deals with the three Cartesian directions, rather than 3N variables in the full many-body wave function.

The foundations of the DFT are based on the two Hohenberg-Kohn theorems [39]. The Honenberg-Kohn Theorems states that the ground state energy of a many-body system is a unique functional of the electron density: $E_o = E[n(\vec{r})]$.The density that yields this minimum value is the exact ground-state density. This theorem allows for the systematic formulation of a many-body problem of interacting electrons in an external potential in terms of the electron density as the basic variable. Using this functional, one may then define, for a given external potential $V_{ext}(\vec{r})$, the energy functional as

$$E[n(\vec{r})] = \langle \Psi | \hat{H} | \Psi \rangle \tag{2.8}$$

In the Honenberg-Kohn representation, the DFT energy functional becomes

$$E[n] = T[n] + E_{Hart}[n] + \int V_{ext}(\vec{r}) n(\vec{r}) d^3\vec{r} + E_{xc}[n] \tag{2.9}$$

where $T[n] = \sum_i \frac{-\hbar^2}{2m_e} < \Psi_i | \nabla_i^2 | \Psi_i >$ is the kinetic energy , $E_{Hart}[n] = \frac{e^2}{2} \iint \frac{n(\vec{r}) n(\vec{r}')}{|\vec{r} - \vec{r}'|} d^3\vec{r} d^3\vec{r}'$ the classical Hartree energy due to electron-electron interaction, $V_{ext}(\vec{r}) = e^2 \iint \frac{n(\vec{r}')}{|\vec{r} - \vec{r}'|} d^3\vec{r}'$ is the external potential due to the nuclei on the electrons (which may include other constant fields) and the last term $E_{xc}[n]$ is exchange and correlation energy.

The electron density can be calculated from the wave function

$$n(\vec{r}) = N \int \cdots \int |\Psi(\vec{r})|^2 d\vec{r}_1 d\vec{r}_2 \cdots d\vec{r}_N \tag{2.10}$$

and

$$\int n(\vec{r}) d^3\vec{r} = N \tag{2.11}$$

where is N is the number of electrons.

The essential quantity of the DFT is the electron density. This theorem states all the characteristics of a system can be calculated implicitly from the density of electrons.

The second theorem states that the energy functional has its minimum at the equilibrium density that is at the exact ground state density $n_o(\vec{r})$. Hence:

$$E[n_o] \leq E[n] \tag{2.12}$$

$$E_o = E[n_o] = \min\{E[n]\}_{n \to n_o} \tag{2.13}$$

The ground state energy may be obtained variationally is that the density that minimizes the total energy is the exact ground state density

$$\left.\frac{\delta E\ [n(\vec{r})]}{\delta n(\vec{r})}\right|_{n(\vec{r}) = n_o(\vec{r})} = 0 \tag{2.14}$$

In this case, the full many particle ground state is a unique function of $n(\vec{r})$. Its form does not depend on the particular system under consideration and $E[n]$ assumes its minimum value for the ground state density with respect to all densities fulfilling Eq. 2.11.

By considering non-interacting electrons, Kohn and Sham [40] expressed how it can formally replace the many-electron problem by an exactly equivalent set of self-consistent one electron equations (single particle theory). It takes into consideration the interaction between electrons via the so-called exchange–correlation functional. The Kohn and Sham total-energy functional for non-interacting electrons can be written as

$$E[\{\Psi_i\}] = \sum_i \frac{-\hbar^2}{2m_e} <\Psi_i | \nabla^2 | \Psi_i > + \frac{e^2}{2} \iint \frac{n(\vec{r}) n(\vec{r}')}{|\vec{r} - \vec{r}'|} d^3\vec{r} d^3\vec{r}$$
$$+ \int V_{ext}(\vec{r}) n(\vec{r}) d^3\vec{r} + E_{xc}[n(\vec{r})] + E_{ion}[\{\vec{R}\}] \qquad (2.15)$$

Here exchange and correlation energies contain, by definition, all the contributions not taken onto account by the first three terms, which represent the kinetic energy functional of the non-interacting electron system, the Hartree and the external energy respectively.

In the Kohn and Sham picture, finding the electron density that minimizes the energy functional is equivalent to solving the set of one particle Kohn and Sham Schrödinger equations. Thus, the ground state can be found by minimizing the set of independent-electron wave functions $\Psi_i(\vec{r})$. It then follows from Eq. 2.15 and Eq. 2.9 that

$$\frac{\delta E[\{\Psi_i(\vec{r})\}]}{\delta \Psi_i(\vec{r})} = \frac{\delta T}{\delta \Psi_i(\vec{r})} + \frac{\delta E}{\partial n(\vec{r})} \frac{\partial n(\vec{r})}{\delta \Psi_i(\vec{r})} = 0 \qquad (2.16)$$

Subjected to the normalization constraints

$$<\Psi_i | \Psi_j> = \delta_{ij} \qquad (2.17)$$

The electron density in terms of a set of one-electron orbitals representing a non-interacting reference system as

$$n(\vec{r}) = \sum_i |\Psi_i(\vec{r})|^2 \qquad (2.18)$$

where the sum runs over the occupied states.

Non-interacting kinetic energy is then determined in terms of the $\Psi_i(\vec{r})'s$ by assuming $T[n] \approx T_o[n]$ whose effect can be included the exchange-correlation term. The Lagrange multiplier method leads to the set of Kohn and Sham Schrödinger-like equations as

$$\left\{-\frac{\hbar^2}{2m}\nabla_i^{\,2}+V_{ext}(\vec{r})+e^2\int\frac{n(\vec{r})}{|\vec{r}-\vec{r}'|}d^3\vec{r}+V_{xc}[n(\vec{r})]\right\}\Psi_i(\vec{r})=\varepsilon_i\Psi_i(\vec{r}) \tag{2.19}$$

with the exchange correlation potential

$$V_{xc}[n(\vec{r})]=\frac{\delta E_{xc}[n(\vec{r})]}{\delta n(\vec{r})} \tag{2.20}$$

where the ε_i's are the eigenvalues and Ψ_i is the one particle wave function. Eq. 2.19 can be rewritten as

$$\left\{-\frac{\hbar^2}{2m}\nabla_i^{\,2}+V_{eff}(\vec{r},[n])\right\}\Psi_i(\vec{r})=\varepsilon_i\Psi_i(\vec{r}) \tag{2.21}$$

where

$$V_{eff}(\vec{r}) = V_{ext}(\vec{r})+\frac{\delta E_{Hart}}{\partial n(\vec{r})}+\frac{\delta E_{xc}}{\partial n(\vec{r})} = V_{ext}(\vec{r})+V_{Hart}[n]+V_{xc}[n] \tag{2.22}$$

Multiplying Eq. 2.19 by $\Psi_i^*(\vec{r})$, using 2.17 and 2.18 gives

$$\sum_i\frac{-\hbar^2}{2m_e}<\Psi_i|\nabla_i^{\,2}|\Psi_i>+e^2\iint\frac{n(\vec{r})n(\vec{r}')}{|\vec{r}-\vec{r}'|}d^3\vec{r}\,d^3\vec{r}'+\int(V_{ext}(\vec{r})+V_{xc}[n(\vec{r})])n(\vec{r})d^3\vec{r}=\sum_1^N\varepsilon_i \tag{2.23}$$

Then final Eq. 2.15, total effective energy functional, using Eq. 2.23 becomes

$$E_{tot}=\sum_{i=1}^N\varepsilon_i-\frac{e^2}{2}\iint\frac{n(\vec{r})n(\vec{r}')}{|\vec{r}-\vec{r}'|}d^3\vec{r}\,d^3\vec{r}'+E_{xc}[n(\vec{r})]-\int n(\vec{r})V_{xc}[n(\vec{r})]d^3\vec{r} \tag{2.24}$$

The above equations are the Kohn and Sham equations that are solved self-consistently. This is the staring point for practical density functional calculations. To summarize, the Kohn and Sham Equations represent a mapping of the interacting many-electron system onto a system of non-interacting electrons moving within an effective potential due to all the other electrons. The single-particle Kohn and Sham

orbitals are constrained to yield the same ground state density as that of the fully interacting system.

The main challenge of DFT is to design the 'functional', or mathematical expressions, to correctly compute the electron density. The exact form of the exchange correlation energy $E_{xc}[n]$ is unknown. There are a number of ways to calculate exchange-correlation energy. Local Density Approximation (LDA) and the Generalized Gradient Approximation (GGA) are the most widely used. The LDA [41] assumes that the exchange correlation energy is only a function of the local charge density of the form

$$E_{xc}[n] = \int n(\vec{r})\varepsilon_{xc}[n(\vec{r})]d^3\vec{r} \tag{2.25}$$

Thereby the exchange-correlation potential becomes

$$V_{xc}[n(\vec{r})] = \frac{\delta E_{xc}[n(\vec{r})]}{\delta n(\vec{r})} = \frac{\delta\{n(\vec{r})\varepsilon_{xc}[n(\vec{r})]\}}{\delta n(\vec{r})} \tag{2.26}$$

One significant limitation of LDA is that under-predicts solids lattice parameters and band gaps while cohesive energies are usually over-predicted.

The other method of approximating the exchange correlation function is the Generalized Gradient Approximation (GGA). The GGA is like the LDA but it considers the gradient of the electron density in addition to the local density. The semi-local functional on the density approximations, a function of the electron density and its derivatives (i.e. the gradient of the electronic density etc), leads to the generalized gradient approximation

$$E_{xc}[n_\uparrow, n_\downarrow] = \int f(n_\uparrow(\vec{r}), n_\downarrow(\vec{r}), \nabla n_\uparrow(\vec{r}), \nabla n_\downarrow(\vec{r}))d\vec{r} \tag{2.27}$$

Exchange correlation potential

$$V_{xc}[n] = \frac{\delta E_{xc}[n]}{\delta n} - \vec{\nabla} \bullet \frac{\partial E_{xc}[n]}{\partial(\nabla n(\vec{r}))} \tag{2.28}$$

The gradient of the density is usually determined numerically. The lattice parameters calculated by GGA generally agree better with experiments than do those from LDA. Nevertheless, there exist many versions of GGA due to the freedom in how to incorporate the gradient term in the exchange correlation energy. In VASP both methods are implemented. Several GGA methods are available including Perdew-Wang (PW) [42, 43] and Perdew-Burke-Ernzernhof (PBE) [41] functional. In this thesis, the PBE approximation was used unless other wise stated. This functional was selected following testing the equilibrium structures, the cohesive energies for silicon bulk crystal and other electronic properties of silicon.

2.6. Basis sets and Pseudopotentials

Having reduced the man-body Schrödinger equations via DFT to one-particle Kohn and Sham Equation, one generally still has to solve the Kohn and Sham equations for a large number of electrons. Calculations can be very much simplified if electrons are divided into two groups: valance electrons and inner electrons. Pseudopotential theory allows one to focus on the chemically active valence electrons by replacing the strong all-electron atomic potential by a weak pseudopotential, which effectively reproduces the potential associated with the core electrons. The core electrons do not take part in chemical reactions and therefore this procedure is acceptable.

The most widely used strategies to solve the Kohn and Sham Equations are to expand orbital wave functions in basis sets of Gaussian orbitals or plane waves. VASP uses plane waves as basis functions and pseudopotentials to represent electron-ion interactions. The expansion of the Kohn and Sham equation using plane waves are discussed (see Appendix A)

VASP provides Vanderbilt ultrasoft (US) [44] and projected augmented wave (PAW) pseudopotentials (PP) [45, 46]. The non-local part of a PP contains a

projected wave function character that can be evaluated in real or **k**-space. The US PP is norm-conserving (NC) while the PAW PP is not norm-conserving. In the norm-conserving pseudopotentials scheme, inside some core radius, the all-electron wave function is replaced by a soft nodeless pseudo-wave function, with the crucial restriction that the pseudo-wave function must have the same norm as the all-electron wave function within the chosen core radius; outside the core radius, the pseudo and all electron wave function are identical [47]. The PAW PPs take advantage of many of the numerical developments of pseudopotential approaches, while retaining information about the core electrons and also representing the valence electron wave functions with their correct nodal form [47].

CHAPTER 3

Computational methods

The following sections describe details of the methods used in simulating the self-directed growth of styrene molecules lines on an incomplete H-terminated Si(100)-2x1 and 3x1 surfaces, and the electronic properties of a silicon surface modified with substituted styrene molecules.

Calculations were performed within the frame work of a periodic density functional theory (DFT) as implemented in VASP [33-36]. The interaction between ions (nuclei) and electrons is described using the projector augmented wave pseudopotentials [46, 48]. Electron–electron exchange and correlation interactions are described using the gradient corrected Perdew-Burke-Ernzerhof (PBE) functional [41].

Initial tests of the electronic properties of bulk Si atom were performed by fitting an equation of state from the plot of the calculated total energy versus the size of the unit cell. Details of the calculation are given in Appendix B. The fit gives a lattice constant of 5.459 Å close to the experimental value of 5.43 Å [49]. Convergences of energy cutoff and k-point meshes were tested. These test indicated that energy cutoff of 384 eV and **k**-point meshes of 11x11x11 are suitable converged results.

The H-Si(100)-2x1 and 3x1 surface were modeled by periodic repeated slabs separated by regions of vacuum into which adsorbed molecules can be added. The molecules are adsorbed on one side of the slab. The bottom silicon layer is terminated by two hydrogen atoms per silicon atom to simulate the tetrahedral coordination of bulk silicon. For the self-directed growth of styrene lines on Si(100) surfaces, the bottom two layers of Si atoms were fixed at the bulk positions. For the electronic properties calculation, the bottom three layers of Si atoms were fixed. The positions of bottom H-caps were also fixed. The remaining layers of silicon and the

adsorbed molecules were allowed to relax to their ground state by minimizing their Hellmann–Feynman forces until all residual forces on the atoms became smaller than 0.02 eV/Å. A uniform **k**-point sampling grid in the surface Brillouin zone with a Gaussian smearing of broadening 0.08 eV [50] was used. The solution of the generalized Kohn and Sham equations is performed using residuum-minimization method by direct inversion in the iterative subspace (RMM-DIIS) procedure [51].

Test calculations were performed by varying the **k**-point sampling grid, broadening parameter, the thickness of the slab (the number of silicon layers representing the substrate) and of the vacuum region in order to ensure that the calculated properties reported in the result and discussion section have converged and that the energy differences are converged within 1meV/atom. For isolated molecules, a large super cell size of 20x20x32 ($Å^3$) and one **k**-point at the gamma center were used. These optimum parameters were used for the simulations presented in this thesis.

3.1. Self-directed growth of one-dimensional (1D) styrene lines

A 2x3 unit cell was used for the H-Si(100)-2x1 surface calculations. A 3x3 unit cell was used for the H-Si(100)-3x1 surface calculations. The 2x3-unit cell consists of six silicon atoms in the surface layer whereas the 3x3-unit cell contains eight silicon atoms. In each case, the slab contains six silicon atomic layers and a vacuum thickness of about 15 Å. An energy cutoff of 400 eV was used for the plane wave expansion. Brillouin-zone integrations using 4×3×1 and 4x4x1 **k**-points Monkhorst–Pack grids were used for the 2x3 and 3x3 unit cells respectively.

Transition state structures were obtained by exploring minimum-energy pathways using the nudged elastic band (NEB) approach [52, 53] implemented in VASP. The energies of the transition states are found by representing a series of images (structures) that interpolate between the initial (reactant) and final (product) states in a particular surface reaction.

Reaction energies and barrier heights obtained using the plane wave approach described in the next sections are not zero-point energy corrected.

3.2. Surface Work function Calculations

For the change in the work function of a clean and hydrogen terminated Si(100)-2x1 surfaces, a slab of eight layers of silicon atoms and a vacuum region of approximately 28 Å was used. The density functional equations were solved using plane wave basis sets with a cutoff energy of 420 eV.

To calculate the work function of organic modified silicon, an asymmetric slab with eight layers of Si atoms and a vacuum thickness of about 26Å was used. The surface had a layer consisting of a variety of para-substituted styrene molecules adsorbed. 2x1 and 4x1-unit cells were used for full monolayer (1 ML) and half monolayer (0.5 ML) coverage, respectively. The work functions of these surfaces without molecules were also calculated. A 2x1 unit cell represents one dimer in a row and contains two silicon atoms in the surface layer. A 4x1 unit cell represents two dimers in two rows and contains four silicon atoms in the surface layer. The bottom layer of silicon atoms and the dangling bonds on the surface are passivated by hydrogen atoms. Dipole correction suggested by Neugebauer [54] has been used in order to avoid interactions between two neighboring super cells along z-axis [100].

For all other calculations, an energy cutoff of 450 eV was used for the plane wave expansion. Brillouin-zone integrations were done using 8×16×1 and 3x15x1 **k**-points Monkhorst–Pack grids for the 2x1 and 4x1 unit cells respectively. The sampling Brillouin zones for other cells reported in Chapter 4 Section 4.2 have been chosen such that they have a similar density of grid points. In this thesis, the work function and the calculated dipole moment are converged within 0.1 eV and 0.1 Debye respectively.

3.2.1. Modeling the structure

In this section, the structures of a variety of para-substituted styrene molecules, 4-X-styrene (Fig. 3.1), adsorbed on H–Si(100)-2x1 are discussed. All molecules adsorbed on the silicon surface were optimized to their minimum ground state energies. This is the important step that links structure and the work function as the work function is highly depending on the position of the molecular dipole array on the substrate. In Fig. 3.1, the different substituted molecules used to create the dipole arrays in the calculations are shown.

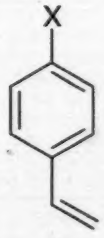

X= $N(CH_3)_2$, NH_2, OCH_3, CH_3, H, COOH, CF_3, OC_2F_3, CN, NO_2

Electron donating groups (EDGs) Electron withdrawing groups (EWGs)

Figure 3.1 The para-substituted styrene (4-X-styrene) molecules considered in the simulations.

Different configurations were used as optimization starting points to find the minimum ground state energy. This was done by rotating the function groups around the benzene ring (ϕ) and by exploring the rotation of the benzene molecule around the plane formed by the atoms C1, C2 and C3 (see Fig. 3.2b). The rotation of 4-X-styrene molecules, Fig. 3.2b, with the normal plane perpendicular to silicon dimer, Si2-Si1-C1-C2 (φ) and the dihedral rotation formed by atoms Si2-C1-C2-C3, (α) were also considered.

The structure of styrene molecules adsorbed via the self-directed growth process on H-Si(100) surface is well established theoretically [11, 21, 22]. The typical structure of the styrene molecular lines on H-Si(100)-2x1 surface is shown in Fig 3.2a. The other substituted styrenes have optimized structures that are very similar as that shown in Fig 3.2. For example the $-CF_3$ and $-CH_3$ functional groups favor the same conformations [55]. The minimum energy structures of the other para-substituted styrene molecules very much resemble that calculated for styrene. However, molecules with $N(CH_3)_2$, OCH_3, CH_3, CF_3 and OC_2F_3 substituents show a large degree of surface disorder at the top of the molecular layer, although their basic backbone (the phenyl and benzyl groups) structure remains similar to that of other para-substituted styrenes.

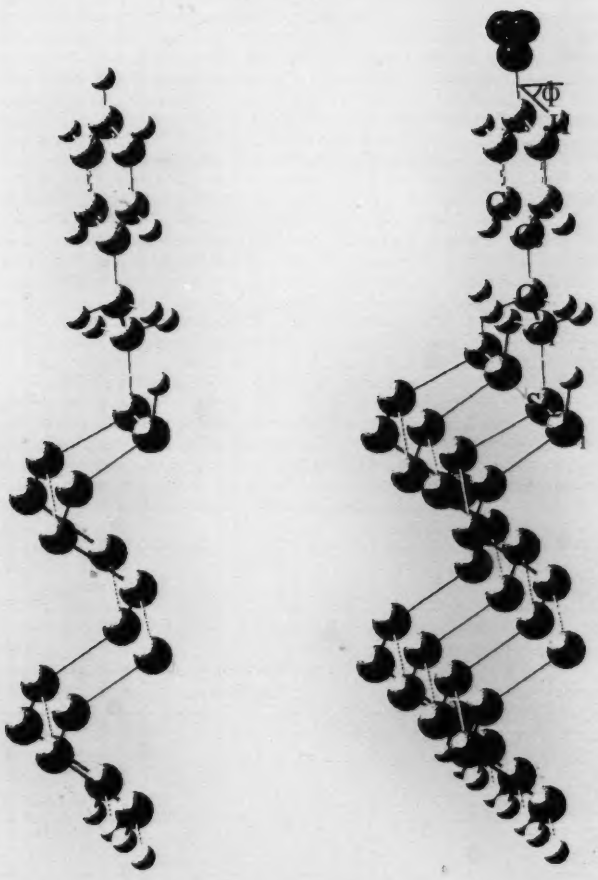

Figure 3.2 Adsorption of styrene molecule on H-Si(100)-2x1 surface (a) unit cell used for 1 ML calculations on a 2x1 unit cell and -NO_2 functional group attached (b) on 4x1 unit cell, 0.5 ML converge.

Fig. 3.2 shows the structure of styrene adsorbed on H-Si(100)-2x1 surface after abstraction of a hydrogen atom from. The optimized structures of the various molecules studied have roughly similar rotational angles (φ), associated with the orientation of the ring with respect to the surface normal. Values of φ for all substituents exhibit variation of $\pm 2^{o}$. However, this angle does not significantly affect the normal of the molecular dipole component and hence they do not affect the work function. The dihedral angles associated with the orientation of the substituents with respect to the ring (ϕ) have the potential to significantly influence

the calculated molecular dipole moment and work function. This is because the degree to which electrons are donated or withdrawn by the substituents depends on how well the groups are conjugated to the benzene ring. The minimum energy structures of all substituted styrenes have a ϕ such that the substituent is maximally conjugated with the ring.

The tilting angle (α) has a large influence on the work function. The work function is sensitive to this normal component. A small tilt angel gives a large normal molecular dipole component which in turn leads a large shift in work function with respect to the clean H-Si(100)-2x1 surface. This is because the component of the molecular dipole moment along the surface normal depends on the tilting angle of the structure according to $\mu_z = |\vec{\mu}|\cos(\alpha)$. However, the optimized structures of all molecules examined have tilting angles (α) that differ by $\pm 3^{o}$. These tilting angle differences are not large enough to change the work function substantially.

In this work, a full ML coverage is defined as one molecule per two surface silicon atoms. It can equivalently be defined as one molecule per dimer. A half ML molecular coverage is defined as one molecule per four surface silicon atoms or one molecule per two dimers. In both cases, all silicon atoms are passivated hydrogen atoms. The geometries associated with full ML and half ML coverage of styrene on H-Si(100)-2x1 are shown in Fig. 3.3.

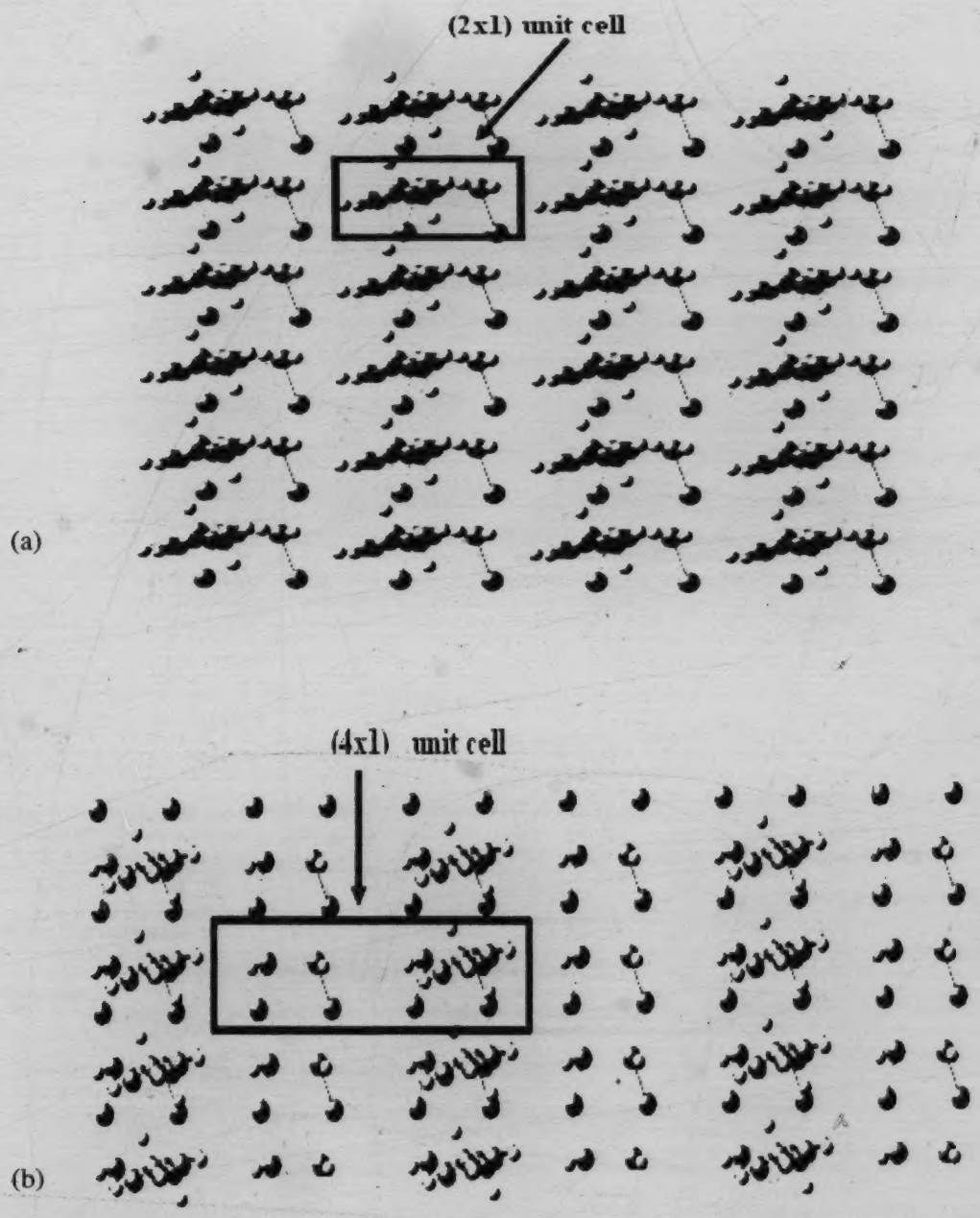

Figure 3.3 Top view of adsorption of styrene molecule on H-Si(100)-2x1 with adsorbed styrene molecules at 1 ML (a) and at 0.5 ML (b) coverage. The 2x1 and 4x1 surface unit cells are indicated by rectangles.

CHAPTER 4

Result and discussion

4.1. Self directed growth of styrene molecules

In this section, two pathways of radical mediated self-directed growth mechanism of styrene molecular lines on an H-passivated Si(100) surface have been studied. The dangling bond at which growth is initiated is placed on a silicon dimer in the H-Si(100)-2x1 and H-Si(100)-3x1 modeling.

4.1.1. Growth on H-Si(100)-2x1 surface

The addition of styrene to the reactive site on H-Si(100)-2x1 is predicted to occur with little or no barrier [56], Fig. 4.1A. The adsorption energy of styrene molecule (the intermediate state) is exoergic by 0.73 eV, indicating that addition of styrene through the C atom to form the intermediate state (Fig. 4.1B) is favourable. The intermediate state can be further stabilized by hydrogen atom abstraction either from the silicon atom in the next dimer in the row through the transition state (TS) shown in Fig. 4.1E or from the silicon atom in the same dimer (via TS Fig. 4.1C). The abstraction of H atom from a neighboring Si dimer takes place via an energy barrier of 0.80 eV. A similar barrier height of 0.83 eV from the silicon atom of the same dimer was obtained.

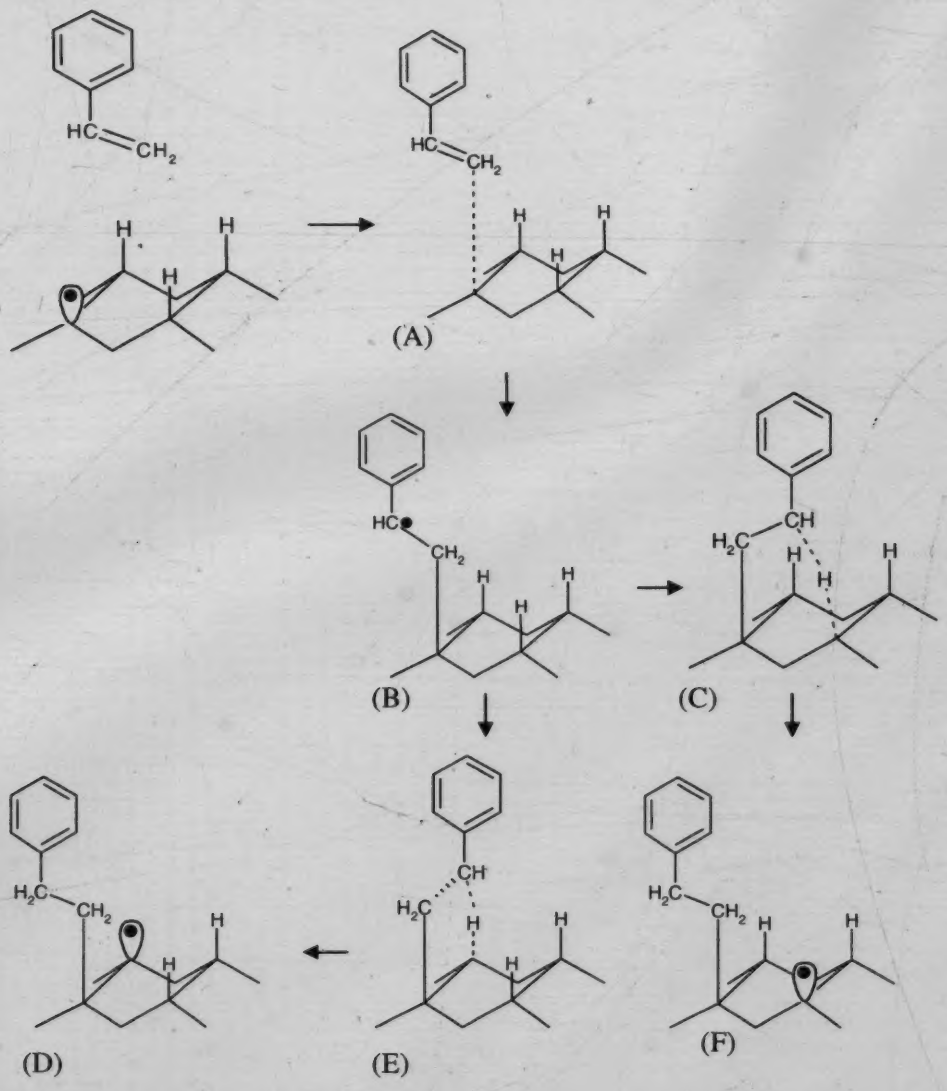

Figure 4.1 Possible reaction pathways for styrene self-directed growth on H-Si(100)-2x1 surface. (A) Styrene molecule approaches a 2x1 surface with a preexisting dangling bond on a dimer row. (B) Styrene molecule adsorption on H-Si(100)-2x1. (C) Transition state for hydrogen abstraction from the same dimer. (D) Final product after hydrogen abstraction from the same dimer. (E) Transition state for hydrogen abstraction from the next dimer. (F) Final product after hydrogen abstraction from the next dimer.

The stability of the carbon centered radical is a key factor for growth of molecular lines; the radical intermediate state for styrene adsorption is stabilized by delocalization of the unpaired electron in the benzyl ring. In general, the magnitude of the intermediate state energy, relative to the separated reactants, is determined by radical delocalization and/or physisorption. If physisorption on the surface is too weak or if the well depth of the intermediate state is too small, desorption of molecules will occur instead of abstracting of a hydrogen atom. For large molecules, weak-noncovalent interactions between molecule and substrate (physisorption) can stabilize the radical species sufficiently for H abstraction to occur [22]. For example, alkenes smaller than 1-heptene do not grow lines, while larger alkenes up to 14 C atoms (for instance 1-undecene) long do grow lines on H-Si(100) [22]. Therefore, dispersion interactions are key for growth to occur. DiLabio et al have demonstrated that large delocalization effects facilitate styrene line growth while longer 1-alkenes are stabilized almost exclusively by dispersion interactions with the surface.

The final states after the abstraction of hydrogen atom from the next (Fig. 4.1D) and the same dimer within the same dimer row (Fig. 4.1F) are lower in energy than the initial reactants by 1.06 and 1.08 eV respectively. The results are given in Table 4.1. These results agree with those obtained from cluster calculations [11, 57]. However, plane wave exoergicity for the addition of styrene to the silicon-dangling bond forming the intermediate state is less than the result obtained by the cluster method by 0.1 eV. Using a cluster approach with a modified B3LYP functional, Musgrave et al [57] showed that the energy barrier height for abstracting hydrogen atom from the same dimer is higher than abstraction of a hydrogen atom from the neighboring dimer by about 0.15 eV [57]. These small differences between the plane wave and cluster methods could be attributed to the level of theory and the methods used in the calculations. Other results such as the barrier height for abstracting a hydrogen atom from the next dimer and the final states obtained using plane wave techniques

agree well with results obtained by Musgrave et al. Other plane wave calculations using LDA and GGA functional forms show the same trend [58, 59]. However, the exoergicity associated with intermediate state formation in the presence work lower than the results reported in other work by 0.17 eV. Other results like the H abstraction barrier from the next dimer and the final states relative to the separated reactants are similar.

Table 4.1 Calculated barrier heights, E_{bar}, and reaction energies, ΔE, for the processes shown in Fig. 4.1.

Process	Reaction	On H-Si(100)-2x1	
		E_{bar}	ΔE^c
Intermediate state	A→B	0.05[a]	-0.73
TS - the next dimer	B→E →F	0.80[b]	-1.08
TS - the same dimer	B→C→D	0.83[b]	-1.06

[a]Addition expected to occur with little or no barrier [56].

[b]Relative to the intermediate states

[c]Relative to the reactants.

There are two possible modes for the growth of styrene molecular lines, which yield either single or double lines. If the H atom is abstracted from the same dimer, a second styrene can bind to the dimer. This second intermediate can then only abstract a H atom from the next dimer in the row. This mode will result in double line formation. The second mode of growth results in the formation of single lines of styrene. This mode occurs when H abstraction occurs exclusively from the next dimer in the row. The plane wave method shows the self-directed growth of the styrene molecular lines on H-Si(100)-2x1 surface along the dimer row occurs almost with the same probability as forming double lines. STM experiments indicate that single styrene lines are observed much more frequently than double lines [11]. It has been shown that benzaldehyde shows different growth patterns of lines on Si(100) [60].

The discrepancy that arises between the plane wave result and the experimental observations could be due to the absence of steric effects in the computational model. The formation of single or double lines likely depends on the presence of preexisting styrene molecules on the surface. However, the present calculations are for only one styrene on the surface. The van der Waals forces between neighboring styrene molecules, will play a role in line growth.

In order to determine if the presence of a preexisting styrene can affect the energetics of line growth, the calculations were repeated for models in which (i) two styrenes were bonded on a single dimer and (ii) two styrenes were bonded to two dimers in one row. In both cases, one of the styrenes was in the intermediate state, analogues to Fig. 4.1B. Unfortunately, the calculations of the H abstraction barrier heights for these models failed to converge. However, calculations indicate that the adsorption of a second styrene on a dimer is exoergic by 0.52 eV. Adsorption of a second styrene on the next dimer is exoergic by 0.49 eV. These exorgicities are lower than that associated with the addition of one styrene on the surface. The differences may be attributed to repulsions between adjacent molecules on the surface.

4.1.2. Growth on H-Si(100)-3x1 surface

Fig. 4.2 shows the potential mechanisms for the reaction of a styrene molecule on the H-Si(100)-3x1 surface. Once again the adsorption of styrene molecule on H-Si(100)-3x1 surface (see Fig. 4.2A) occurs via an almost barrierless process. The adsorption of styrene molecules on the reactive site of the silicon surface (see Fig. 4.2B) is exoergic by 0.68 eV and reaction of styrene through the C atom is favourable. This adsorption energy is slightly lower than that obtained on 2x1 surfaces likely due to steric effects. In this case, there is a smaller separation between the dimers and monomer rows on the 3x1 surface than between two dimer rows on the 2x1 surface. The intermediate state can be further stabilized by hydrogen atom abstraction from the silicon next dimer row (Fig. 4.2E), from the

silicon atom within the same dimer (Fig. 4.2D) or from the silicon in the monomer row (Fig. 4.2C).

Of the three mechanisms considered (Fig. 4.2C, D, E) for the abstraction of hydrogen atom on H-Si(100)-3x1 surface, the computational results indicate that the abstraction of a H-atom from the monomer is the most likely to occur (see Table 4.2). The abstraction of an H atom from an adjacent monomer (Fig. 4.2C) has an energy barrier of 0.48 eV, which is small as compared to the other processes. The barrier for this using cluster method is 0.55 eV [61]. The energy barrier height to abstract hydrogen from the same and next dimer are 0.76 eV and 0.80 eV respectively. These energy barrier heights are little lower than those obtained on the 2x1 surface. The results are consistent with the experimental observations that growth will occur across the dimer row on the H-Si(100)-3x1 surface.

Table 4.2 Calculated barrier heights, $E_{bar,}$ and reaction energies, ΔE, for the processes shown in Fig. 4.2.

Process	Reaction	On H-Si(100)-2x1	
		E_{bar}	ΔE^c
Intermediate state	A→B	0.05[a]	-0.68
TS - monomer	B→C →F	0.48[b]	-0.77
TS - the same dimer	B→D →G	0.76[b]	-1.03
TS - the next dimer	B→E →H	0.80[b]	-1.01

[a]Addition expected to occur with little or no barrier [56].

[b]Relative to the intermediate states

[c]Relative to the reactants.

The overall exoergicity following the abstraction of hydrogen atom from the next dimer in the row and the same dimer within the dimer row (see Fig. 4.2G and 4.2H) are 1.03 and 1.01 eV, respectively. However, exoergicity following abstraction of hydrogen atom from the monomer row is lower than the other processes by 0.24-

0.26 eV (see Table 4.2). The difference arises from the Si-H bond energy on the monomer compared to that of the dimers. Calculations reveal that the Si-H bond energy on the dimer row is weaker by 0.21 eV than the Si-H bonding energy on the dihydride monomer. There may be additional but small contributions from steric effects. As a result, the final product after abstracting hydrogen atom from the monomer site is energetically less stable than that from the dimer row. This reaction is therefore kinetically controlled, meaning that it is controlled by the path with the lowest barriers as opposed to the path associated with the largest energy release.

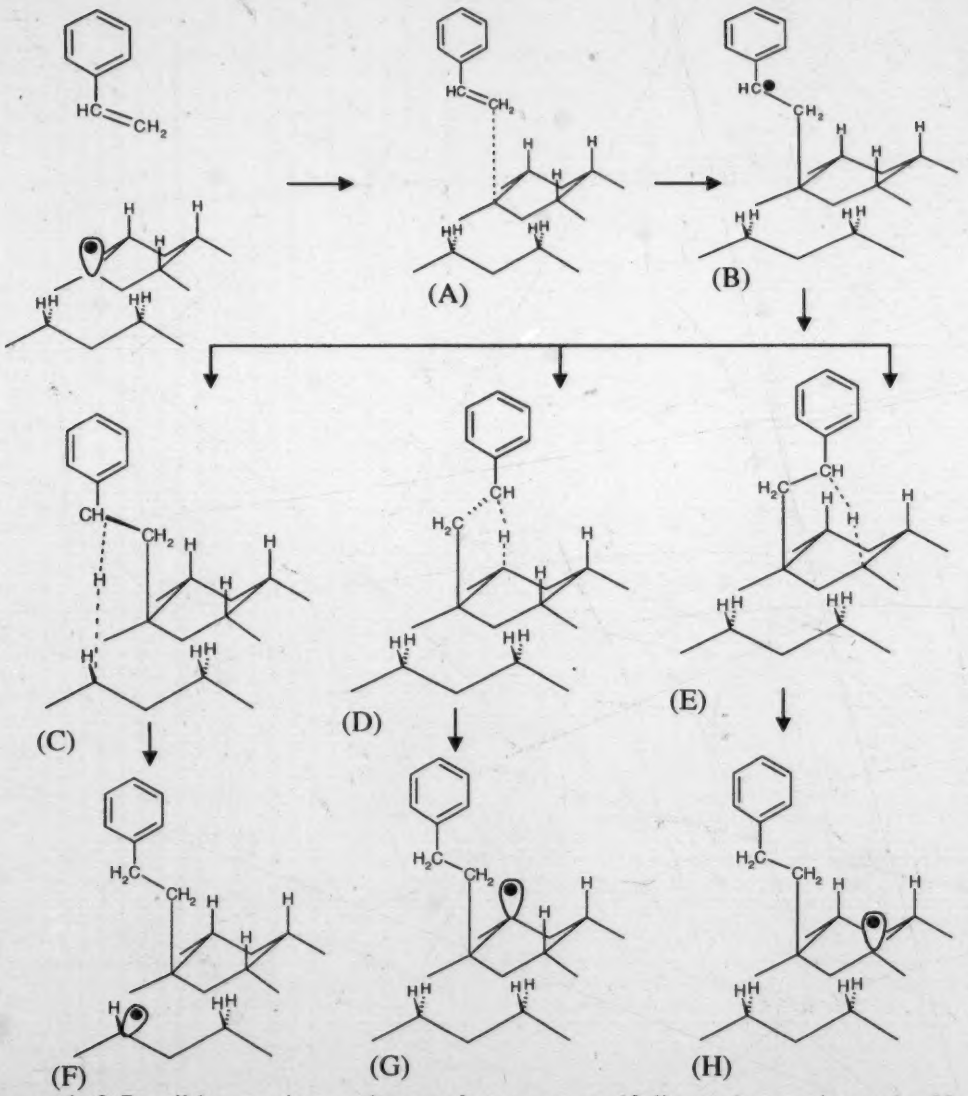

Figure 4. 2 Possible reaction pathways for styrene self-directed growth on the H-Si(100)-3x1 surface. (A) Styrene molecule approaches a 3x1 surface with a preexisting dangling bond on a dimer row. (B) Styrene molecule adsorption on an H-empty site. (C) Hydrogen abstraction from the monomer row. (D) Hydrogen abstraction from the same dimer. (E) Hydrogen abstraction from the next dimer along the row. (F) Final product after hydrogen abstraction from the adjacent monomer site. (G) Final product after hydrogen abstraction from the same dimer. (H) Final product after hydrogen abstraction from the next dimer.

These findings are consistent with the observation by STM and with the results of cluster calculations [61]. In the final state after the hydrogen atom abstraction from the adjacent monomer, the hydrogen atom left on the dihydride site (Fig. 4.2F) flips on the other side (closer to the styrene) within the dihydride site through an inversion of the silicon center.

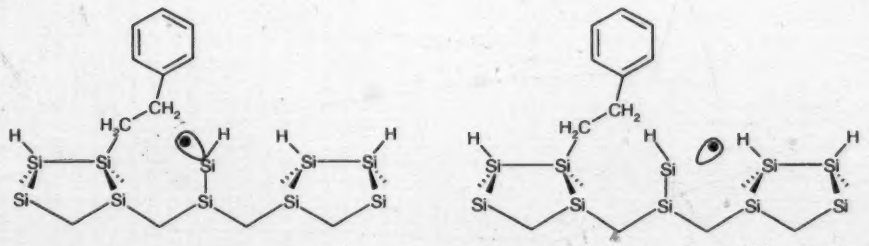

(a) (b)

Figure 4.3 The proposed mechanism of styrene chain reaction on H-Si(100)-3x1 surface in the cross-row direction. (a) Final state after abstraction of an H atom from the adjacent monomer. (b) Inversion of H atom on the monomer site.

The flipping of hydrogen atom shown in Fig. 4.3 is quite facile and moves the dangling bond closer to the next dimer row. An H atom from the neighboring dimer row is able to diffuse to the monomer ($\Delta E \approx 0.24$ eV) thereby moving the dangling bond to the dimer row for the chain reaction to continue.

The details of the H-atom diffusion processes were not studied as part of the work in this thesis. The energy barriers for the diffusion processes are available in the literature [61].

To summarize the results, the self-directed growth mechanisms of styrene molecular lines on Si(100) surface using plane wave DFT-PBE calculations were investigated. Calculations predict that styrene molecules could grow equally well along the dimer

row (to form single line) or same dimer (to form double lines) on the 2x1 surface. This does not agree with the experimental findings that line growth occurs almost exclusively along one side of dimer row. Subtle effects like steric hindrance play a role in such discrepancy. On the 3x1 surface, calculations predict that line growth occurs in the perpendicular to row direction. The mechanism involves abstraction of H atom from the monomer site can be followed by flipping of hydrogen within the monomer site. Diffusion of the hydrogen atom from the dimer row to the empty site of the monomer site can then occur, allowing growth to continue in the direction that is perpendicular to dimer rows. These findings are in full agreement with experimental observations.

4.2. Work function changes with 4-X-Styrene molecular functionalization of H-Si(100)-2x1

The modification of semiconductor surfaces using organic molecular ensembles whose properties can be changed using a simple synthetic procedure is a versatile way to change the electronic properties of the substrate. The aim of this section is to understand how the adsorption of different organic molecules, with accompanying variation of molecular dipole moment, alters the work function of a Si Surface. There are presently no experimental data on the work function change of H-Si(1001)-2x1 upon the adsorption of para-substituted styrene molecules with which to compare. However, recent scanning tunneling microscopy observations indicate that local changes in work function occur when different molecules are adsorbed on H-Si(100)-2x1. For example, 4-OCH_3-styrene and 4-CF_3-styrene liner hetrostructures under different biasing voltages display a reversal in height contrast [62]. A similar behavior is also observed for 4-CF_3-styrene and styrene hetrostructures. These observations indicate that surface dipole moments across the hetrostructures alter the STM current flow. Changes in the direction and magnitude of the dipole moment cause the tunneling current to switch on at different biases. Vilan et al [30] have also observed a similar behavior for molecules on a metal surfaces.

The work function change for a chemisorbed system is associated closely with the direction and the magnitude of electron transfer, changes in the surface dipole moment, the charge rearrangement associated with bond formation around the interface between the substrate and the adsorbate and image charge on the substrate (particularly for conducting surfaces). In the present model, the image charge effect on the substrate will not be considered as such treatment requires substantial computation resources and is expected to have minimum effect in the non-metallic system under study. In this section, the effect of molecular dipole moment (an ordered dense-packed array) on the electronic properties of the surface, specifically on the work function, is studied. The self-directed growth by radical chain reaction, as it has been discussed in Section 4.1, can potentially generate an ordered organic monolayer of styrene on an otherwise hydrogen terminated surface The effects of both electron donating and withdrawing groups attached chemically at the head of styrene molecule have been examined.

The work function is the minimum energy required to take an electron from the solid to the vacuum level outside the surface. The work function is obtained by subtracting the Fermi energy of the system from the electrostatic potential in the middle of the vacuum gap

$$\Phi = V_{vac} - E_f \qquad (4.1)$$

where V_{vac} is the electrostatic potential in the vacuum at a distance where the microscopic potential has reached its asymptotic value within a few angstroms from the surface and E_f is the Fermi energy of the system. Note that the asymptotic value of the electrostatic potential will be higher that the value obtained at infinity because of the surface dipoles.

A self-consistent electronic structure calculation using a plane wave basis set produces the electrostatic potential $V(\vec{r})$ on a grid in real space, which is the sum of the Hartree potential, $V_{Hart}(\vec{r})$, and the ion-electron pseudopotential, $V_{pp}^{local}(\vec{r})$

$$V(\vec{r}) = V_{pp}^{local}(\vec{r}) + V_{Hart}(\vec{r}) \tag{4.2}$$

The average and the smoothed electrostatic potential in the surface normal along the z-axis [100] direction can be obtained using

$$\overline{V}(z) = \frac{1}{L}\int_{z-L/2}^{z+L/2} dz' \frac{1}{A}\iint_{cell} V(x, y, z')dxdy \tag{4.3}$$

where A is the area of the surface unit cell normal to z [100] and L is the distance between the substrate layers. If the vacuum thickness is large enough, the vacuum potential reaches its asymptotic value around the middle of the vacuum level.

To get the work function according to Eq. 4.1, one needs an accurate value of the Fermi energy inside the material. For semiconductor material, H-Si(100)-2x1, the Gaussian broadening smearing value (0.08 eV) and the **k**-point sampling are varied to place the Fermi level around the midgap of the conduction and valence bands. Once these parameters are determined, they were used for the rest of adsorbed-substrate calculations. The Fermi energy level can also be obtained from the adsorbed-substrate slab calculation quite reasonably if a slab of sufficient thickness is used. The DFT computational results obtained using the above method give work functions converged to within 0.1 eV.

4.2.1. Full monolayer coverage (X= OCH_3 , CH_3 , H, COOH, CF_3)

4.2.2.1. Clean and hydrogen terminated Si(100)-2x1 surfaces

As a reference, the work functions of clean and H-terminated Si(100)-2x1 were calculated. The results of these calculations will provide some perspective on the quality of the result that can be obtained by modeling.

(a) (b)

Figure 4.4 Schematic representation of (a) the buckled dimer in the Si(100)-2x1 surface and (b) dimer in the hydrogen terminated Si(100)-2x1 surface.

On the clean Si(100) surface, the silicon atoms pair up to give the (2x1) dimerized reconstruction geometry resulting in a π-bond between each silicon atom in the dimer. However, surface dimers on the Si(100)-2x1 surface are buckled as a result of asymmetric charge distribution on the geometry (Fig. 4.3a). Because of the asymmetric charge distribution, Si atoms become slightly negative (δ^-) and positively (δ^+) charged. When this surface is exposed to hydrogen atoms, each silicon dangling bonds will bind by one hydrogen atom resulting a monohydride Si(100)-2x1 surface, shown in Fig. 4.3b. Adsorption of atomic hydrogen on the reconstructed 2x1 surface removes the asymmetry of the dimer bonds.

The calculated buckling height difference and tilt angle of the dimer are 0.68 Å and 16.44° respectively, which are very similar to those values obtained for the (2x2) structure (0.66 Å and 15.9°) [63]. The change in the work function of a clean (buckled) surface and hydrogen terminated Si(100)-2x1 surface are calculated and

compared with published experimental results. A 2x2-unit cell is used in which each unit cell includes two adjacent dimers along a dimer row as illustrated in Fig. 4.4.

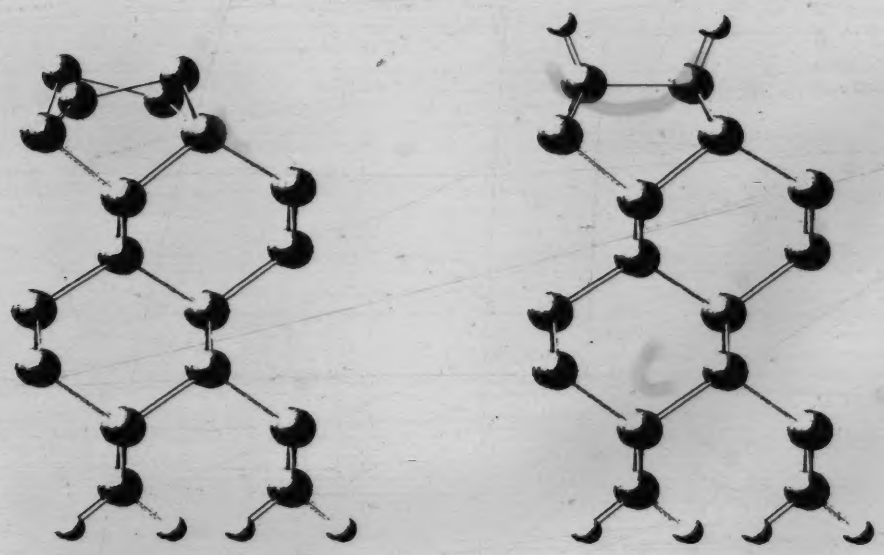

(a) (b)

Figure 4.5 A 2x2 surface unit cell of the (a) Si(100)-2x1 surface and (b) H-Si(100)-2x 1 surface used in the calculations.

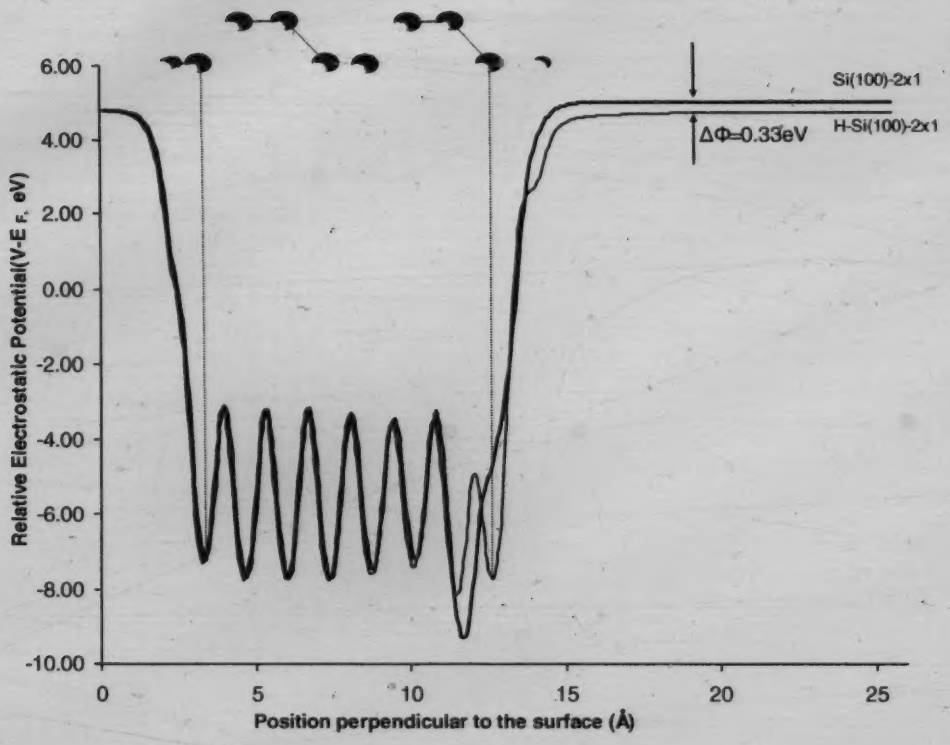

Figure 4.6 An averaged relative planar electrostatic potential of a clean Si(100-2x1 and H-Si(100) surface as a function of position [100] direction. The Fermi energy is set to zero, V-E_F. The inset shows a "Ball and Stick" representation of the surface. The vertical lines correlate the position of the bottom and the top silicon atomic layers with the electrostatic potential.

Fig. 4.6 shows the relative planar averaged electrostatic potential as a function of position in the [100] direction. The direction is perpendicular to the surface and through the vacuum. The blue and the red lines represent the calculated planar averaged electrostatic potential for the clean and hydrogen terminated Si(100)-2x1 surface, respectively. The inset "Ball and Stick" line represents positions of atoms. The ends (white ball) represent the bottom and the top hydrogen terminated layers while in between are the positions of the silicon atomic layers. Each silicon atomic

layer is separated by 1.34 Å. The average planar electrostatic potential from 4 to 15 Å represents that of the silicon layers. The troughs correspond to the planar averaged electrostatic potential of the silicon atomic layer (marked in broken line). Above 15 Å are the asymptotic electrostatic potentials of the clean Si(100)-2x1 (blue) and the hydrogen terminated Si(100)-2x1 (red) surfaces. The plot shows that the work function is shifted to a lower value for H-Si(100)-2x1. For a full monolayer of hydrogen terminated silicon surface, the work function is calculated to be 4.63 eV. For the clean Si(100)-2x1 surface , the calculated work function is 4.96 eV, which compares well to other theoretical values which range from 4.88-4.96 eV [64]. Thus at a full H coverage on the 2x1 surface, the change in the work function is computed to be 0.33 eV. This work function change is comparable to the experimental values which range from 0.30-0.45 eV [65-67]. These results therefore provide some confidence with respect to the prediction of the work function change.

The reduction in the work function upon H-termination can be attributed to the reduction in the surface dipole moment. On the clean 2x1 surface, the surface has an asymmetric charge distribution in which one of the Si atoms becomes slightly positive and the other becomes partially negatively charged. This creates an electric dipole moment on the surface as compared to the unreconstructed clean Si(100) surface, Si(100)-1x1. Thus, a higher work function is observed as compared to an ideal and the H-terminated surfaces. Adsorption of atomic hydrogen on the reconstructed 2x1 surface removes the asymmetry of the dimer bonds; no asymmetric charge distribution on the surface is formed.

The change in the work function at hydrogen coverage of 0.5 ML and 0.75 ML were also calculated. At 0.5 ML hydrogen coverage, one of the silicon atoms in a dimer is capped by hydrogen atom. At 0.75 ML hydrogen coverage, three silicon atoms in two dimers in two rows are capped by hydrogen atoms. These are the surfaces used for organic molecule adsorption calculations, which are discussed in the next section. The work function for 0.5 ML hydrogen coverage is 4.73 eV while the

work function for 0.75 ML hydrogen coverage is 4.67 eV. These values are very close to the work function of full H-terminated of Si(100)-2x1 surface. Similarly, the work function of the full hydrogen terminated tetrahedral bulk silicon (4.68 eV) on the bottom of the slabs used in modeling is close to that of the full hydrogen terminated Si(100)-2x1 surface. Despite different structures and different degree of H termination, all of these surfaces have very similar work functions. Therefore, it appears that dipole associated with buckling on the clean surfaces is responsible for the difference in the work function between the clean and hydrogen terminated surface. From this point forward, the Si(100)-2x1 surfaces with any degree of hydrogen terminated will be denoted by H-Si(100)-2x1 in the context of discussion of work function.

4.2.2.2. Change in work function of the H-Si(100)-2x1 surface with 4-X-Styrene adsorption

The change in work function due to one monolayer (1 ML) coverage of 4-X-styrene on the otherwise H-terminated Si(100)-2x1 is discussed in this section. For this work, X=OCH_3, CH_3, H, COOH and CF_3. The number of functional groups studied is extended in the work on 0.5 ML coverage described in Section 4.2.2.

In the previous section, it has been shown that adsorption of hydrogen on the clean Si(100)-2x1 surface reduced the work function by 0.33 eV from 4.96 eV to 4.63 eV, in good agreement with experimental results [65, 67]. The work function for H-Si(100)-2x1 surface is taken as a reference point. The change in the work function of Si(100)-2x1 surface $\Delta\Phi$ upon the adsorption of molecules is calculated as

$$\Delta\Phi = \Phi_{mod} - \Phi_{H\text{-}Si(100)\text{-}2x1} \qquad (4.4)$$

where Φ_{mod} is the modified work function of the surface after the adsorption of molecules and $\Phi_{H\text{-}Si(100)\text{-}2x1}$ is the unmodified work function of the H-Si(100)-2x1.

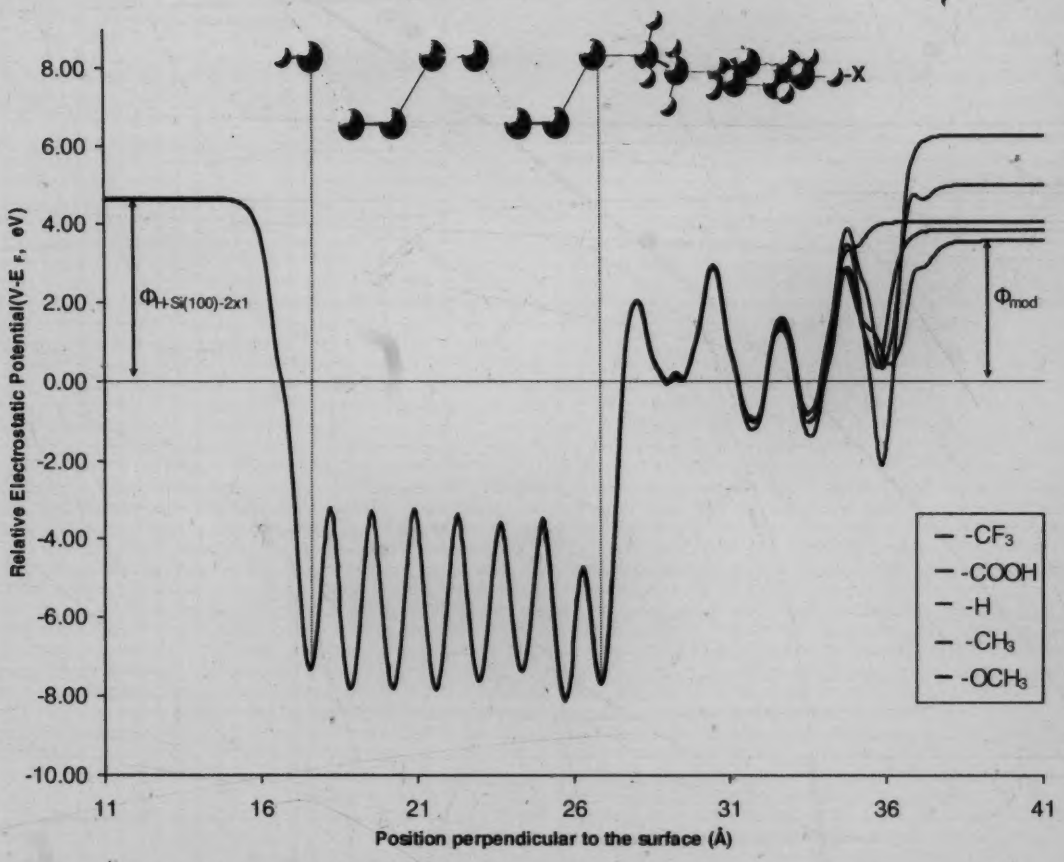

Figure 4.7 Planar averaged electrostatic potential for 1 ML coverage of different aromatic molecules adsorbed on H-Si(100)-2x1 as a function of position, in the direction perpendicular to the surface. The left side represents the work function of H-Si(100)-2x1, and the right side represents the modified work function of the surface upon the adsorption of 4-X-styrene molecules, written on the plot. The Fermi level is set to zero. The inset shows a "Ball and Stick" representation of the silicon atomic layers and molecules. The vertical lines show the position of the bottom and the top silicon atomic layers. X denotes where the substituents are placed.

The plot in Fig. 4.7 shows the planar averaged electrostatic potential for different aromatic molecules adsorbed on H-Si(100)-2x1 as a function of slab position in the direction perpendicular to the surface along the vacuum direction. The Fermi level is set to zero. The average planar electrostatic potential from 0 to 15 Å is constant and represents the potential for the H-Si(100)-2x1 surface without the adsorption of molecules. The electrostatic potential from 15 to 28 Å represents that of silicon atomic layers (see inset). The electrostatic potential from 28 to 36 Å is that of the molecular layers of substituted styrene. These molecules are dipole arrays. Above ~36 Å, the space above the molecules in the vacuum, represents the work function of the modified H-Si(100)-2x1 surface upon the adsorption of molecules. As can be seen, the left side or unmodified surface (without the adsorption of molecules) is the same for all molecules whereas the variation on right side strongly depends on the substituents on the styrene molecules.

The origin of the work function change, $\Delta\Phi$, as a function of X can be interpreted in terms of change in the surface dipole upon adsorption of the molecules. If the adsorbed molecules are well oriented, parallel and close-packed, then they can be considered as a dipole layer and a uniform electrostatic potential change must occur over the width of the layer. To get a better understanding of this phenomenon, in the next section the surface dipole moment is decoupled into two parts, the contribution from molecular dipole moment of the monolayer and the dipole moment formed at the interface due to the chemical bonding between the adsorbed molecules and the surface (chemisorption dipole moment).

4.2.2.3. Deconvoluting the Surface Dipole by examining the molecular and chemisorption contribution to $\Delta\Phi$

The section focuses upon the distribution of the surface dipole moments in the molecular MLs and the chemisorption dipole moment components. The work function change, $\Delta\Phi$, can be interpreted in terms of change in the surface dipole, $\Delta\mu$, due to adsorption of the molecules, see Fig. 4.8a. Classical electrostatics,

according to the Helmholtz Equation, gives the change in the work function, $\Delta\Phi$, upon the adsorption of a dense ML adsorption as

$$\Delta\Phi = \frac{e\mu\cos(\theta)}{\varepsilon_o A} = \frac{e\mu_z}{\varepsilon_o A} \tag{4.5}$$

where ε_o is the permittivity of vacuum and A is the surface area taken by one molecule in a full monolayer, $\mu_z = \mu\cos(\theta)$, is the change in surface dipole that occurs upon adsorption of the molecules normalized per molecule, and θ is the average titling angle of the adsorbed molecule from the surface normal. Note that μ_z corresponds to the component of the dipole moment directed along the surface normal, since this is the only component that effects the work function.

To get insight into the origin of the change in the work function, a method suggested by Michaelides et al [68] is also applied to calculate the change in the surface dipole moment μ_z induced by the adsorption of molecules. The surface dipole moment can be calculated at any arbitrary plane, z, inside the structure by integrating the electron density within the slab with respect to the vacuum as [69, 70]

$$\mu_z(z) = \int_z^{z_{cell}} (z'-z)\rho(x,y,z')dxdydz' \tag{4.6}$$

where μ_z represents the dipole moment between the vacuum and the plane z. The quantity $\rho(\vec{r})$ is the charge density and Z_{cell} is the super cell size in the vertical direction. For 4-X-styrene molecules with X = OCH_3 and CF_3, the magnitude surface dipole calculated using Eq. 4.6 are 0.93 and 1.29 Debye respectively. These results are in good agreement with values of 0.89 and 1.27 obtained using Eq. 4.5. Since, Eq. 4.5 is easier to use, only those results obtained using expression 4.5 are reported.

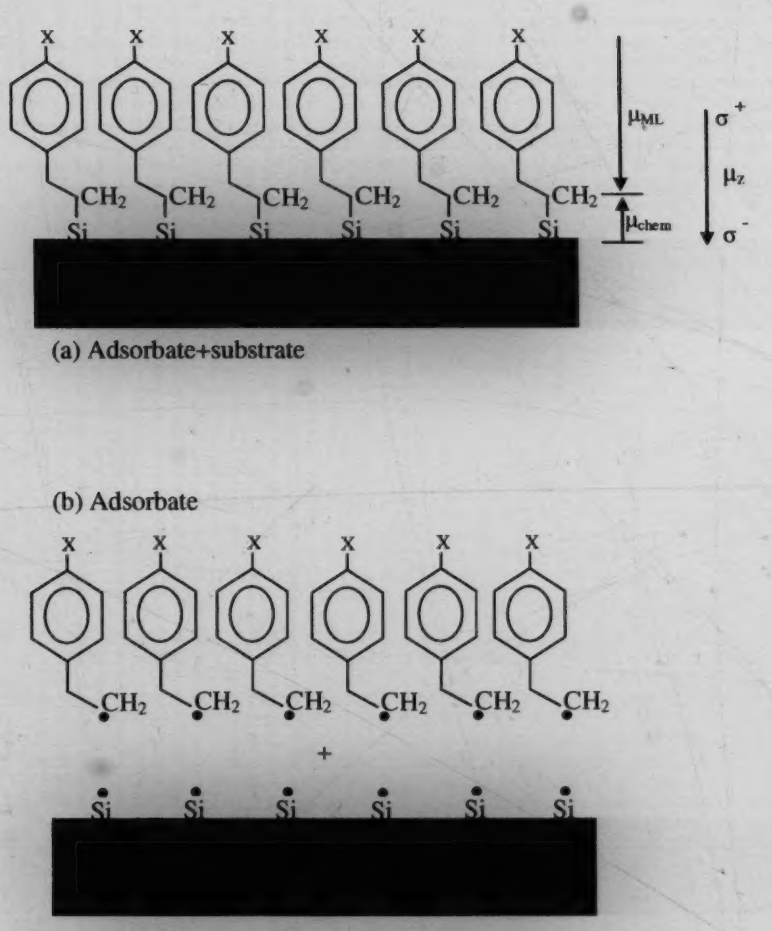

Figure 4.8 Schematic representations of modification of a silicon surface with an organic molecular layer. (a) Molecular layer on a surface. (b) A molecular monolayer is formed in the same geometry as it was in (a). (c) An H-Si(100)-2x1 surface with half H monolayer coverage. Arrows indicate the direction of the surface dipole moment, molecular and interface dipole moments. For example for EDGs, charge density per unit area created in the monolayer is indicated, σ^+ and σ^-. X denotes where the substituents are placed.

Fig. 4.8 shows a schematic representation of the silicon surface and molecular layers adsorbed on the surface used in the calculations. To evaluate the two components of

the surface dipole, in Fig. 4.8a, the adsorbate+substrate is divided into two parts, the adsorbate molecular layer (Fig. 4.8b) and silicon substrate (Fig. 4.8c). This method helps us to determine the dipole moment contribution due to the molecular layers and due to chemisorption. The monolayer is considered as a dipole sheet whose sides are negatively or positively charged. For example, for the EDGs, the charge density per unit area created in the monolayer is indicated as σ^+ and σ^-. The dipole moment is directed from the positive to the negative site. Under such conditions, the surface dipole is considered as an infinite two dimensional dipole layer. The surface dipole moment can be divided into two as a molecular and interface dipole moment created across the interface between the C and Si atoms.

One can express the surface dipole moment μ_z from the contribution of molecular dipole moment and the dipole moment created through the charge transfer that accompanies chemical bond formation between the molecule and the surface. This can be written as

$$\Delta\Phi = \frac{e\mu_z}{\varepsilon_o A} = \frac{e(\mu_{ML} + \mu_{chem})}{\varepsilon_o A} \qquad (4.7)$$

where μ_{ML} is the dipole moment of the molecular ML along the surface normal of a molecule as depicted in Fig. 4.8b, i.e. without the presence of the silicon substrate and μ_{chem} is the dipole moment due to the charge transfer upon chemisorptions. One can directly determine the change in the work function from the sum of the shift in the vacuum level of the molecular layer (ΔV_{ML}) and the shift due to bond formation.

Computationally, the geometry of the molecular layer used for these evaluations is the same geometry as it was embedded in a unit cell of the adsorbate-substrate system as illustrated in Fig. 4.8. DFT calculations were performed on the ML geometry as it was optimized when on the H-Si(100)-2x1 surface. Using the

Helmholtz principle, one can then relate molecular dipole moment μ_{ML} to the steps in the electrostatic potential across the molecular layer as

$$\Delta V_{ML} = V_{right} - V_{left} = \frac{e\mu_{ML}}{\varepsilon_o A} \tag{4.8}$$

where V_{right} *and* V_{left} are the asymptotic electrostatic potentials on both sides of the molecular layer. These values can be obtained from the asymptotic potentials within a few angstroms of either side of the molecular layer (see Fig. 4.9).

For a closely packed layer of molecules, the effect of molecular dipole moment surrounding each molecule in the molecular layer, at full monolayer coverage, is taken into account as an effective dielectric constant in the molecular layer in the periodic boundary conditions DFT calculations. If the molecules are close enough (very densely packed), then there will be a charge transfer between the molecules or charge rearrangement within the molecule so as to reduce the electric fields. i.e. the effect of the depolarizing electric field.

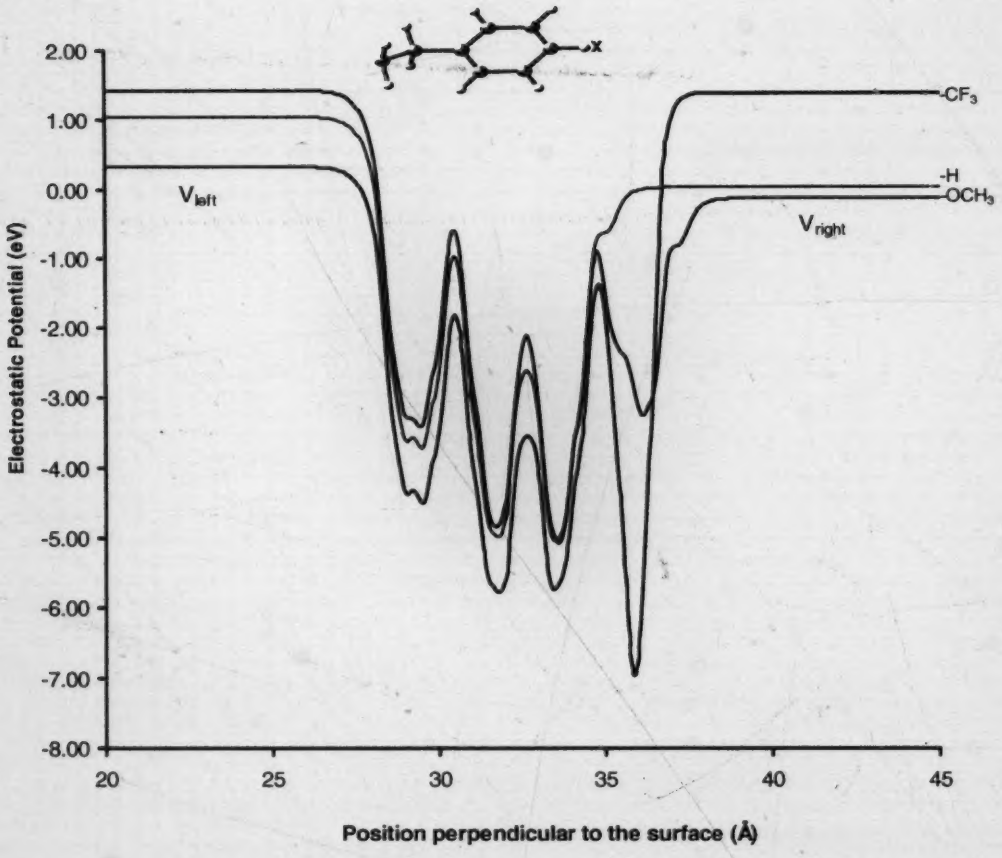

Figure 4.9 Plane averaged electrostatic potential of styrene and para-substituted styrene molecular layers perpendicular to the surface as a function of the position inside the unit cell. The inset shows a "Ball and Stick" representation of the molecule.

Fig. 4.9 shows is the planar average electrostatic potentials across molecular layers as a function of position in [100] direction as illustrated in Fig. 4.8b. The left side of the plot represents the asymptotic potential of the molecular layers (directed to the surface) and the right side is the asymptotic potential along the direction of the dipole arrays. The electrostatic potential for other molecular layers (not shown here) are similar.

Table 4.3 Step in vacuum electrostatic potential ΔV_{ML} across the molecular layer, left and right ionization potentials (IP_{left} and IP_{right}) of the layers of molecules and molecular dipole (μ_{ML}) of the layers at full coverage for 4-X-syrene. X denotes the substituents

X	ΔV_{ML} (eV)	IP_{left} (eV)	IP_{right} (eV)	μ_{ML}(Debye)[a]
OCH_3	-1.56	5.23	3.67	-1.25
CH_3	-1.21	5.28	4.07	-0.97
H	-1.02	5.27	4.25	-0.81
COOH	-0.02	5.24	5.22	-0.01
CF_3	1.02	5.25	6.27	0.87

[a]Calculated using Eq. 4.8

The results in Table 4.3 show the step in the electrostatic potential across the molecular layer obtained from the difference in the left and right sides of the asymptotic electrostatic potential plot shown in Fig. 4.8 for substituted styrene. The left side and the right side of the ionization potential (IP) energies of the molecular layer are obtained by subtracting the highest occupied molecular orbital (HOMO) level of the molecular layer from the left and right sides of the asymptotic electrostatic potentials respectively. The value of IP depends on which side of the ML electron comes from because the electron comes from the HOMO of the monolayer (constant) but the electrostatic potential differs depending on which side the electron is ejected to. This is the result of having an infinite monolayer and is directly analogous to the work function. The left side of the ionization potential energy of the molecular layer is the same for all substituents whereas the right side depends on the nature of the substituents. Molecules with electron withdrawing groups (EWGs) have larger IP_{right} values as compared to styrene, where as molecules with electron donating groups (EDGs) have lower IP_{right} values. This is consistent with experimental ΔIP ((4-X-C_6H_4 -$CHCH_2$) - (4-H-C_6H_4 -$CHCH_2$)) values. For example for X=CH_3, ΔIP =0.26 eV [71] which is in good agreement

with ΔIP_{right} =0.18 eV, Table 4.3. Note that free molecules have one IP, the IP for an isolated molecule on the left and right side are the same. This is because, for free molecules, the electrostatic potentials on all sides converge to the same value at infinity. Finite layers also give the same IP for the left or right sides.

Because of the variation in ΔV_{ML} with the electron donating and withdrawing strength of the substituent, the molecular dipole moment μ_{ML} calculated using Eq. 4.8 strongly depends on the substituents. The sign of μ_{ML} is such that for EDGs the dipoles point from the substituent molecule into the benzene ring, whereas for EWG point from the ring into the substituent.

Table 4.4 Change in the work function ($\Delta\Phi$(eV)) of an H-Si(100)-2x1 upon the adsorption of 4-X-syrene, surface dipole (μ_z), molecular dipole (μ_{ML}) and the chemisorption dipole moment (μ_{chem}) and Fermi energy (E_F) at full monolayer coverage. Dipole moments are in Debye.

X	$\Delta\Phi$ (eV)	μ_z[a]	μ_{ML}[b]	μ_{chem}[a]	E_F (eV)
OCH_3	-1.12	-0.89	-1.25	0.35	-1.62
CH_3	-0.84	-0.67	-0.97	0.30	-1.77
H	-0.63	-0.50	-0.81	0.31	-1.87
COOH	0.32	0.26	-0.01	0.27	-2.12
CF_3	1.60	1.28	0.87	0.41	-2.53

[a]Calculated using Eq. 4.7. [b]Calculated using Eq. 4.8.

Table 4.4 summarizes the changes in the work function of H-Si(100)-2x1 surface upon the adsorption of a variety of para-substituted styrene molecule at 1 ML coverage, the surface dipole moment, the molecular dipole moment and the chemisorption dipole moment. The result shows the dependence of the shift in the work function upon the substituents. The interface dipole moment, which is due to bond formation, is fairly constant for all substituents. The charge transfer in the

adsorption of molecules occurs mainly in the formation of the covalent Si-C bond. This charge transfer is about 0.35 electron/bond. The bond formation between Si and C atoms is a σ bond; the electrons are localized as compared to the delocalized π-electron in the ring. The charge transfer in a single σ bond is not affected by the ring substituents, which are far away. This is consistent, for example, with the fact that C-H bond strengths in substituted toluenes are relatively constant [72]. The results obtained at 1 ML coverage show that EDGs such as CH_3 and OCH_3 on vinyl benzene molecules lower the work function by 0.84 and 1.12 eV respectively, whereas the EWGs COOH and CF_3 increase the work function by 0.32 and 1.60 eV respectively. This is a direct result of the dipole arrays in the molecular monolayer. The electric dipole layer resulting from the EDGs pulls electrons to the surface, making it easier to eject an electron. The electric dipole layer resulting from the EWGs pushes electrons away from the surface, making it harder to eject an electron.

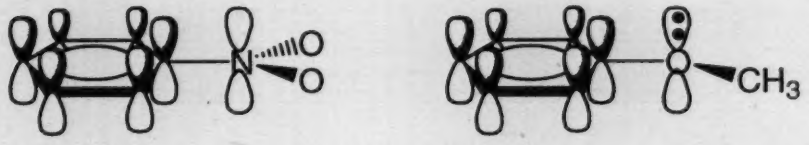

(a) (b)

Figure 4. 10 Conjugation between π-type molecular orbital of the functional groups (a) NO_2 and (b) OCH_3 with the ring.

The dipole moment created by substituents can be understood in terms of electron density transfer between the ring and the substituents. Large dipole moment is created if the substituent is maximally conjugated with the ring in addition to electron density transfer upon bond formation. For the EWGs such as NO_2, the electron density is transferred from the ring to the NO_2 through two mechanisms, (i) through the polar C-N σ bond and (ii) via the conjugation between an empty π-type molecular orbital of the functional group and π molecular orbital of the ring [73]. In the case of EDGs, for example in OCH_3, electron density is transferred from the

ring to the substituent through the polar C-O σ bond. However, the dominating effect of the electron donation results from the overlap of a doubly-occupied p-type orbital on the O atom and the ring of π orbitals.

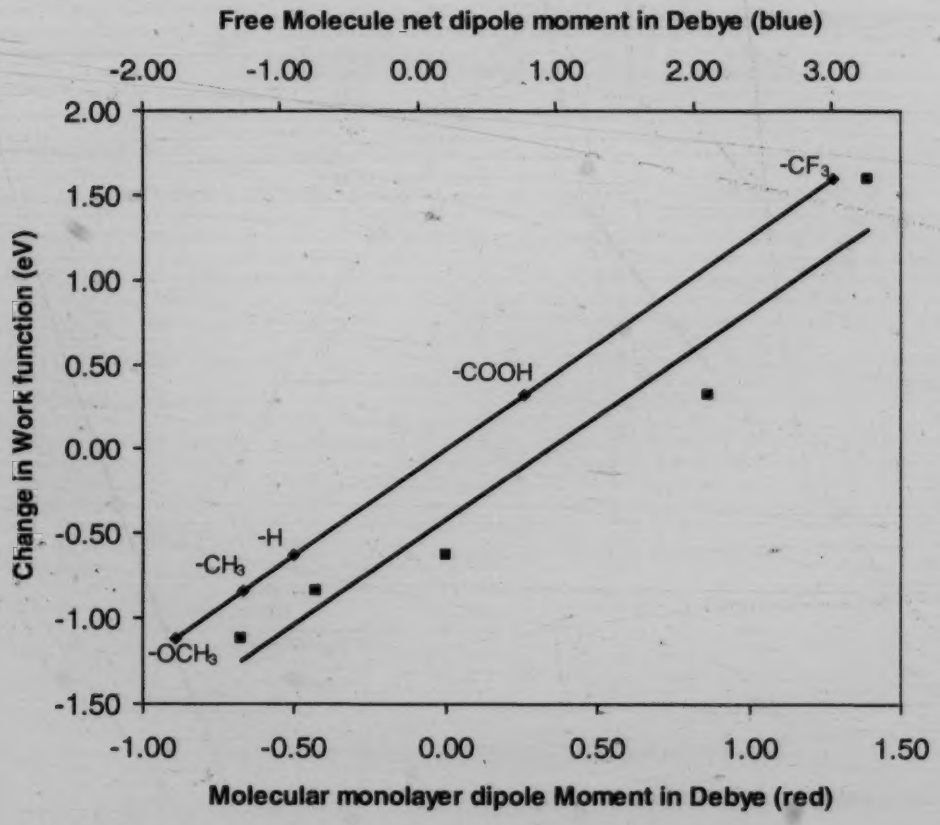

Figure 4.11 Change in work function with molecular dipole moment (σ = 0.89 and R^2 =1.00) and free molecule net dipole moment (σ = 1.92 and R^2 =0.94) at full ML coverage. Substituents are indicted.

Fig. 4.11 shows the calculated work function shift depends linearly on the molecular monolayer and correlates well with the net dipole of the isolated molecules. Linear behavior is not observed in the change in work function versus the dipole moment of free molecule because the dipole moment plotted is the net norm dipole moment

of the free molecule. Only the component of the dipole moment of the free molecule perpendicular to the surface changes the work functions.

4.2.2.4. Charge transfer at the interface between organic molecular layer and Si surface

Chemisorption often causes large change in the observed work function. This is because there is usually a high degree of charge transfer between the adsorbate and the surface when strong chemical bonds are formed. For example, one can predict that the adsorbates that have a higher electronegativity with respect to the surface will have the opposite effect on the work function compared to adsorbates that have a lower electronegativity.

When molecules are adsorbed on the surface, there will be a redistribution of electrons in the interface region between the surface and the molecule. A full understanding of the different behavior of the work function change on H-Si(100)-2x1 requires close examination of the electron density differences. To get a better view, the planar averaged electron density difference $\Delta\rho(z)$ along the z direction for styrene and trifluoromethyl styrene MLs adsorbed on H-Si(100)-2x1 surface is plotted, Fig. 4.12.

The electron density difference $\Delta\rho(\vec{r})$ is obtained by subtracting the densities of the clean substrate $\rho_{Sur}(\vec{r})$ and the molecular layer $\rho_{Adsor}(\vec{r})$ from the density of the adsorbate-substrate system $\rho_{Sur+Adsor}(\vec{r})$ as illustrated in Fig. 4.8.

$$\Delta\rho(\vec{r}) = \rho_{Sur+Adsor}(\vec{r}) - \rho_{Sur}(\vec{r}) - \rho_{Adsor}(\vec{r}) \qquad (4.9)$$

This quantity gives insight into the redistribution of electrons upon the adsorption of different organic molecules.

Having calculated μ_z and μ_{ML} using Eq. 4.5 and 4.8, μ_{chem} can be easily calculated using Eq. 4.7. Results at 1 ML and 0.5 ML coverage are given in Table 4.4 and 4.5. From these, we see that the contribution of μ_{chem} to the surface dipole due to a variety of para-substituted styrene molecules is more or less the same for all kinds of substituents.

One can also get this result from the charge density difference using Eq. 4.6 by only replacing $\rho(z)$ by $\Delta\rho(z)$ and integrating. Nevertheless, the change of surface dipole moment induced by molecule-surface interaction at the interface is complicated. In general, it cannot be estimated simply as a product of the charge transferred and the distance between molecule and the surface. Considering the charge transfer from the surface to the molecules, the simple picture of electrons being transferred from the surface to molecules cannot easily be found in the planar plot (Fig. 4.12). In general, determination of an accurate dipole moment due to charge transfer around the interface is complex, and only be done using the difference in the surface dipole moment and molecular dipole moment (Eq. 4.7).

When an atom/molecule adsorbs on a surface two phenomenon occur. If the ionization energy (IP) of the adsorbate is lower than the work function of the substrate, electron density will be transferred from the adsorbate to the substrate. This transfer takes place until the chemical potential reaches the same value. This electron density transfer to the surface results in a positive charge on the adsorbate. The resulting effective dipoles are in the opposite direction to those of the clean surface and these counteract surface dipole layer, resulting in a reduction in the work function.

If the IP of the adsorbate is greater than the work function of the surface, then the adsorbate withdraws electron density from the surface. The electron transfer from the surface to the adsorbate results in a positive charge on the substrate and a negative charge adsorbate. The resulting effective dipole is in the same direction to

that of the clean surface, enhancing the surface dipole layer, and increasing the work function.

In this study, as we see in Table 4.4, the IP of the adsorbed molecular layers is greater than the work function of the silicon surface regardless of the substituent. Charge transfer occurs from the surface to the molecular layer until the chemical potential of the Si(100)-2x1 surface and the molecular layer reaches the same value.

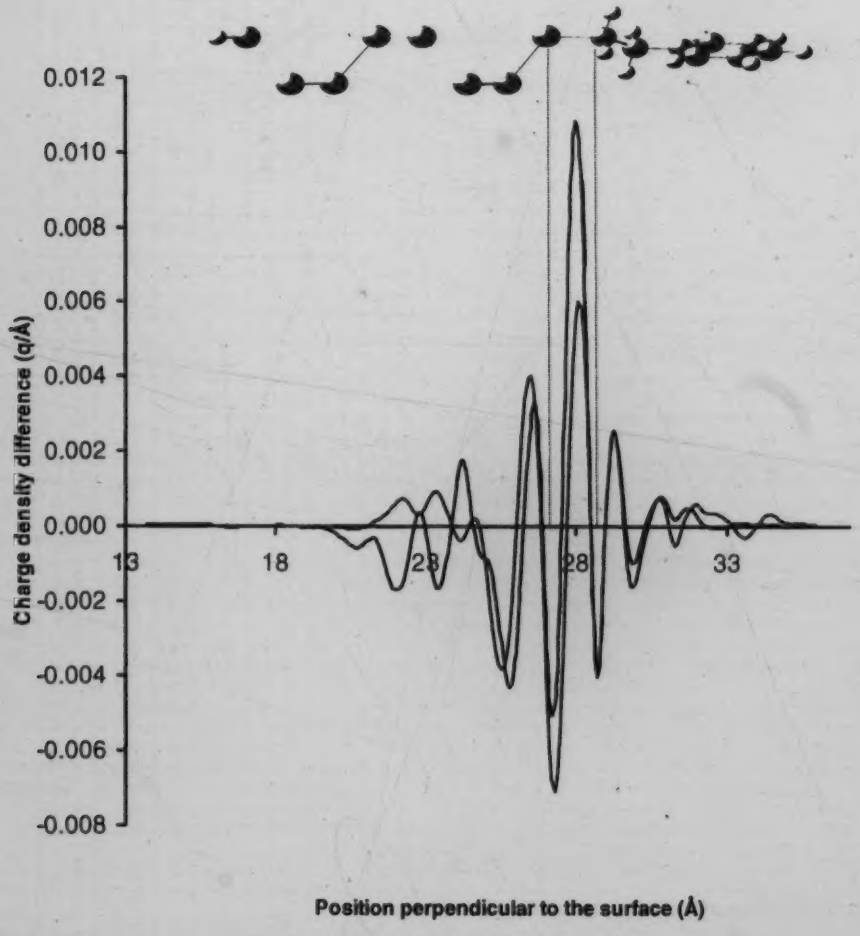

Figure 4.12 Planar averaged electron density differences for CF_3-Styrene (blue) and styrene (red) ML on an H-Si(100)-2x1 surface. Both are the functions of z, the direction perpendicular to the surface. The inset shows a "Ball and Stick"

representation of the silicon atomic layers and molecules. The vertical lines show the position of the top Si and the bottom C atoms.

Fig. 4.12 is the planar averaged electron density difference for styrene (red) and CF_3-Styrene (blue) molecular layers adsorbed on the silicon surface as a function of position to illustrate the charge redistribution in the interface (the silicon substrate and the adsorbed molecular layers). It is obtained by calculating the charge densities of each component depicted in Fig. 4.8 using Eq. 4.9. The charge density difference for other substituents not shown in the above plot gives the same as CF_3-Styrene. The change in the charge density difference, charge rearrangement, within the first few layers of silicon surface is the result of substituents.

As we see in Table 4.3, the left side of ionization energy of the molecular layer is greater than the work function of both the clean and the hydrogen terminated silicon surface and hence there is an offset between the molecular IP and the work function of H-Si(100)-2x1 surface. This results in charge transfer from the substrate to 4-X-styrene molecule until their Fermi levels reach equilibrium. The amount of charge transfer is fairly constant for all molecular layers and substituents. There is some charge rearrangement around the CH_2-CH_2 groups and the top silicon layer. The charge redistribution decays within the first four-silicon layers and within the benzene ring.

When two atoms with different electronegativity form a σ-bond, there is some charge transfer. The electron transfer from silicon to carbon atom was calculated. This was done by taking the electron density difference from the position where the silicon atom begins and the carbon atom ends. It turns out that for all molecules, the magnitude of the electron transfer is within ±0.005e upon the change in substituents. This is consistent with the fact that the substituents do not significantly change the μ_{chem}. These dipole arrays only create a charge rearrangement within the benzene ring and the first few layers of silicon surface as illustrated in Fig. 4.12.

The simple picture of electronic charge transfer from the substrate to the adsorbate upon bond formation does not completely describe the change in work function. It is the molecular dipole moment of the organic molecules directed on the substrate significantly changing the observed work function shift.

To summarize, as we see in Fig. 4.10, the change in the work function is linearly correlated with both the isolated molecules and the molecular dipole moment of at 1 ML coverage.

4.2.2. Half monolayer coverage(X= $N(CH_3)_2$, NH_2 , OCH_3 , CH_3 , H, COOH, CF_3, OC_2F_3, CN , NO_2)

One can expect the shift in the work function upon adsorption variety of para-substituted styrene on H-Si(100)-2x1 surface to depend upon the packing density of the molecules (coverage) and the ionization potential of the adsorbed molecular layer. The coverage dependence relates to the packing density of molecular dipoles and the depolarizing effect. The methods applied in the previous section are also applied to half monolayer coverage in order to study the coverage dependence of the calculated change in work function.

Table 4.5 Change in the work function ($\Delta\Phi$(eV)) of an H-Si(100)-2x1 upon the adsorption of 4-X-syrene, surface dipole (μ_z), molecular dipole (μ_{ML}), the chemisorption dipole moment (μ_{chem}) and the Fermi energy (E_F) at half monolayer coverage. Dipole moments are in Debye.

X	$\Delta\Phi$	μ_z[a]	μ_{ML}[b]	μ_{chem}[a]	E_F (eV)
$N(CH_3)_2$	-1.37	-1.10	-1.29	0.20	-0.91
NH_2	-1.43	-1.14	-1.33	0.19	-1.15
OCH_3	-0.72	-0.57	-0.75	0.17	-1.48
CH_3	-0.54	-0.43	-0.58	0.15	-1.61
H	-0.41	-0.33	-0.47	0.15	-1.67
COOH	0.33	0.26	0.12	0.14	-1.81
CF_3	0.99	0.79	0.65	0.14	-1.92
OC_2F_3	1.51	1.21	1.06	0.15	-1.99
CN	1.86	1.49	1.29	0.20	-2.31
NO_2	1.85	1.48	1.35	0.13	-2.14

[a]Calculated using Eq. 4.7. [b]Calculated using Eq. 4.8.

Table 4.5 summarizes the change in the work function of H-Si(100)-2x1 surface upon the adsorption of a variety of para-substituted styrene molecule at 0.5 ML coverage, which includes the surface dipole moment, the molecular dipole moment and the chemisorption dipole moment. Comparing the data in Tables 4.4 and 4.5, the work function change depends on both the coverage and surface dipole moment. Comparing the results at different coverage, the chemisorption dipole moment at 0.5 ML coverage is less than the result obtained at 1 ML coverage. This is a direct consequence of the amount of charge transfer per unit area associated with chemical bonding formation. The dipole moments of the molecular layers at 1 ML and 0.5 ML coverage are quite different. For instance, for substituents OCH_3 and CF_3 the magnitude of molecular dipole moments are 1.25 and 0.87 Debye, and 0.75 and 0.58 Debye at 1 ML and 0.5 ML coverage, respectively. This is a result of the packing density of the electric dipole layer sheet. As we see from Table 4.4 and 4.5, the

change in the work function for COOH terminal group at half and full coverage turns out to be similar. This can be attributed to the surface dipole moment, which is calculated to be the same for both 1 ML, and 0.5 ML coverage. The IP_{left} and IP_{right} of the molecular layer is also the same in both cases. This predicts that smaller doses of 4-COOH-styrene molecules on Si(100)-2x1 are enough to fully change surface electronic properties. The other feature observed in the simulations is the alignment of the molecular HOMO level with respect to the Fermi level. In all cases, the HOMO level of the adsorbed molecular layer is found with the same shift below the Fermi level regardless of the substituents. That means the ΔE_{HOMO}-E_F is constant. This can be attributed to the charge transfer across the molecular layer, which is the same for all substituents.

One can expect the shift in the work function upon adsorption of a variety of para-substituted styrene on H-Si(100)-2x1 surface to depend upon the packing density of the molecules and coverage. The higher value of the work function at 1 ML coverage relates to the packing density of the adsorbates. However, increasing the packing density of the molecular dipoles increases the depolarizing field of the molecular layer. This in turn decreases the molecular dipoles due to the interaction among molecules. However this effect is small.

The effects of the packing density in this model, at 0.5 ML and 1 ML coverage, on the work function shift can be seen from the results (Table 4.4 and 4.5). At lower coverage, a small shift in the work function of the modified surface is obtained as compared to at the higher coverage. In general, the coverage dependence relates to the packing density of molecular dipoles/surface dipoles. The variation of the molecular IP, on the other hand, relates to the substituents.

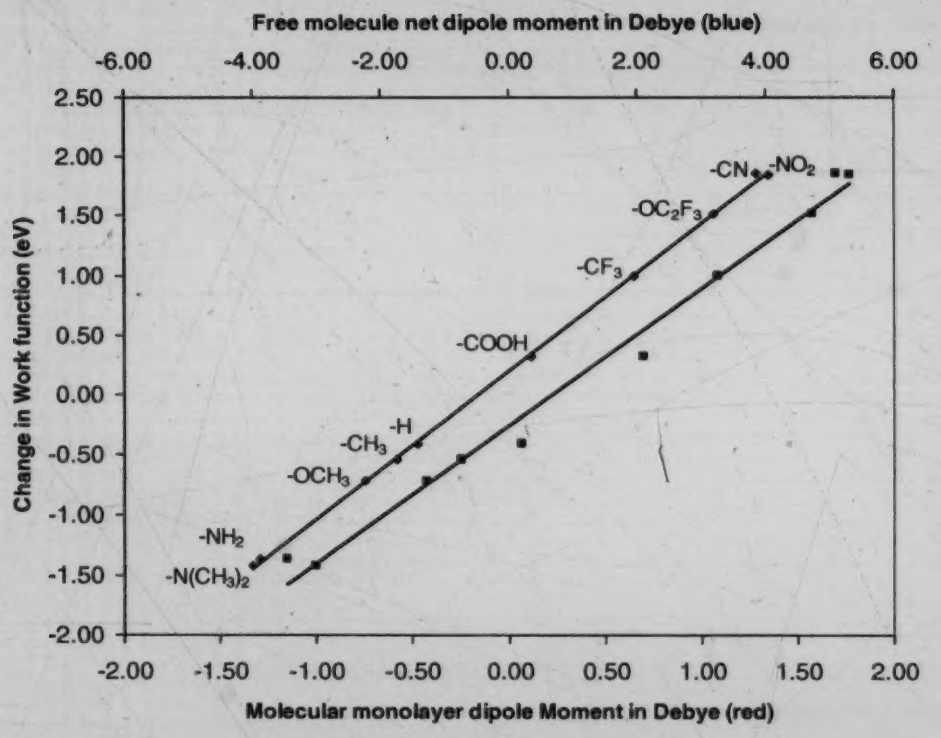

Figure 4.13 Change in work function with molecular dipole moment (σ = 1.03 and R^2 =1.00) and free molecule net dipole moment (σ = 3.33 and R^2 =0.98) at 0.5 ML coverage.

The above plot shows how the molecular dipole moment of the adsorbed molecules correlates linearly with change in the work function of the surface at the 0.5 ML coverage. It also shows the linear correlation between the changes in the work function of the surface with the net norm dipole moment of the free isolated molecules. As we see from the plot, the calculated work function shift depends linearly on both the molecular and the net dipole moments of the free molecules.

To summarize, the surface dipole moment reproduce well in the change in work function on the H-Si(100)-2x1 surfaces upon organic molecular ML adsorptions. It has been shown that the work function shift for all structures can be attributed to a

larger normal component of the molecular dipoles (dipole layers), see Table 4.4 and 4.5. Though the bonding between the molecule and the surface contributes to the work function shift, results here are virtually the same for all organic molecules studied as compared to the styrene molecular layer. In other words, the magnitude of the dipole moment due to the charge transfer between the adsorbate and the silicon surface is the same within 0.14 Debye. The small variation can be attributed to the structure of the geometry of the dipole arrays in the simulation, normal surface dipole, and consequently work function is sensitive to the tilt angle of the molecule as stated in Chapter 3. For example, calculations show that a very small shift in any of the atoms/molecules within the unit cell results in a change in the chemisorption dipole moment by about 0.1 Debye.

Therefore, the work function change results because of the molecular dipole moments of different dipole arrays. The interface dipole moment due to charge transfer upon bond formation is the same for all substituents studied.

CHAPTER 5

Conclusions

In summary, using the first principle DFT calculations, the self-directed growth formation mechanism of molecular lines on Si(100) surface using PBE functional form were investigated. Several possible H-atom abstraction pathways were taken into account. As a result, the plane wave methods shows styrene molecules grow equally both along the dimer row and within the dimer to form single or double lines on the H-Si(100) surface. However, experimental observations revealed that styrene molecules grow more frequently along the dimer row in the 2x1 surface. The discrepancy that arises between the plane wave result and the experimental observations could be due to the absence of steric effects in the computational model On the other hand, on the H-Si(100)-3x1 surface, styrene molecules grow across the dimer row, which is consistent with the experimental observations. In general, the plane wave DFT method using the PBE exchange functional predicts results that are consistent with experimental observations.

Electronic properties, particularly the work function modification of the surfaces, were also studied. The chain reaction mechanism of styrene and para-substituted styrene molecules were considered to form molecular monolayers on the hydrogen terminated Si(100)-2x1 surface. The surface dipoles and work functions of different organic molecules with functional groups ($N(CH_3)_2$, NH_2, OCH_3, CH_3, COOH, CF_3 , OC_2F_3, CN and NO_2) chemically attached at the head group of styrene molecule on the Si(100)-2x1 surface by means of DFT calculations were studied. It has been shown that the electronic properties of the Si(100)-2x1 surface can be tuned by modifying adsorbate organic molecular monolayer properties using different functional groups. Separate calculations were done for the freestanding of the molecules as it was on the H-Si(100)-2x1 surface. The properties of the molecular layer were calculated such as the vacuum level shift, the molecular dipole moment and the ionization potentials. This method allows to calculate the dipole

moments that result from charge transfer across the interface between the adsorbate molecules and Si surface. From this, it has been found that the amount of the charge transfer due to the substituent turns out to be similar to the charge transfer between the styrene molecule and Si surface. The above electronic properties were studied at full and half monolayer coverage. The shift in the work function is a result of the change in the surface dipole moment, which is the sum of the molecular and the chemisorption dipole moments. At 0.5 ML and 1 ML coverage, the work function change correlates linearly with the molecular dipole moment normal to the surface and net dipole moment of the free molecules. However, the work function shifts due to the charge transfer is the same and can be taken as a constant.

The direction of these effects is such that adsorption of 4-X-styrene (X = $N(CH_3)_2$, NH_2, OCH_3, CH_3, H) lowers the work function as compared to the clean Si(100)-2x1 surface, whereas adsorption of 4-X-styrene (X = COOH, CF_3, OC_2F_3, CN , NO_2) increases the work function. This work function shift is also correlated with the coverage of the surface. Therefore, by varying the reactivity of a particular adsorbate, control of the surface electronic properties can be achieved.

Bibliography

[1] J. M. Buriak, *Chemical Communications* **1999**, 1051-1060.

[2] J. M. Buriak, *Chemical Reviews* **2002**, *102*, 1271-1308.

[3] A. B. Sieval, R. Linke, H. Zuilhof and E. J. R. Sudholter, *Advanced Materials* **2000**, *12*, 1457-1460.

[4] D. D. M. Wayner and R. A. Wolkow, *Journal Of The Chemical Society-Perkin Transactions 2* **2002**, 23-34.

[5] R. A. Wolkow, *Annual Review Of Physical Chemistry* **1999**, *50*, 413-441.

[6] S. F. Bent, *Surface Science* **2002**, *500*, 879-903.

[7] N. P. Guisinger, N. L. Yoder and M. C. Hersam, *Proceedings Of The National Academy Of Sciences Of The United States Of America* **2005**, *102*, 8838-8843.

[8] R. J. Hamers, *Nature* **2001**, *412*, 489-490.

[9] M. Ratner, *Nature* **2005**, *435*, 575-577.

[10] M. R. Linford, P. Fenter, P. M. Eisenberger and C. E. D. Chidsey, *Journal Of The American Chemical Society* **1995**, *117*, 3145-3155.

[11] G. P. Lopinski, D. D. M. Wayner and R. A. Wolkow, *Nature* **2000**, *406*, 48-51.

[12] J. Yoshinobu, H. Tsuda, M. Onchi and M. Nishijima, *Journal Of Chemical Physics* **1987**, *87*, 7332-7340.

[13] J. T. Yates, M. J. Bozack, P. A. Taylor and W. J. Choyke, *Abstracts Of Papers Of The American Chemical Society* **1986**, *192*, 159-COLL.

[14] W. Pan, T. H. Zhu and W. T. Yang, *Journal Of Chemical Physics* **1997**, *107*, 3981-3985.

[15] C. Mui, S. F. Bent and C. B. Musgrave, *Journal Of Physical Chemistry A* **2000**, *104*, 2457-2462.

[16] P. W. Loscutoff and S. F. Bent, *Annual Review Of Physical Chemistry* **2006**, *57*, 467-495.

[17] W. Widdra, C. Huang, S. I. Yi and W. H. Weinberg, *Journal Of Chemical Physics* **1996**, *105*, 5605-5617.

[18] R. E. Schlier and H. E. Fransworth, *Journal Of Chemical Physics* **1959**, *30*, 917.

[19] J. L. Reddinger and J. R. Reynolds in *Molecular engineering of pi-conjugated polymers, Vol. 145* **1999**, pp. 57-122.

[20] S. W. Lee, L. N. Nelen, H. Ihm, T. Scoggins and C. M. Greenlief, *Surface Science* **1998**, *410*, L773-L778.

[21] P. G. Piva, G. A. DiLabio, J. L. Pitters, J. Zikovsky, M. Rezeq, S. Dogel, W. A. Hofer and R. A. Wolkow, *Nature* **2005**, *435*, 658-661.

[22] G. A. DiLabio, P. G. Piva, P. Kruse and R. A. Wolkow, *Journal of the American Chemical Society* **2004**, *126*, 16048.

[23] W. Monch, *Journal Of Vacuum Science & Technology B* **1989**, *7*, 1216-1225.

[24] P. S. Bagus, V. Staemmler and C. Woll, *Physical Review Letters* **2002**, *89*.

[25] X. Crispin, V. Geskin, A. Crispin, J. Cornil, R. Lazzaroni, W. R. Salaneck and J. L. Bredas, *Journal Of The American Chemical Society* **2002**, *124*, 8131-8141.

[26] S. R. Lunt, G. N. Ryba, P. G. Santangelo and N. S. Lewis, *Journal Of Applied Physics* **1991**, *70*, 7449-7465.

[27] S. Bastide, R. Butruille, D. Cahen, A. Dutta, J. Libman, A. Shanzer, L. M. Sun and A. Vilan, *Journal Of Physical Chemistry B* **1997**, *101*, 2678-2684.

[28] R. Cohen, L. Kronik, A. Shanzer, D. Cahen, A. Liu, Y. Rosenwaks, J. K. Lorenz and A. B. Ellis, *Journal Of The American Chemical Society* **1999**, *121*, 10545-10553.

[29] I. G. Hill, A. Rajagopal, A. Kahn and Y. Hu, *Applied Physics Letters* **1998**, *73*, 662-664.

[30] A. Vilan, A. Shanzer and D. Cahen, *Nature* **2000**, *404*, 166-168.

[31] S. Park, T. U. Kampen, D. R. T. Zahn and W. Braun, *Applied Physics Letters* **2001**, *79*, 4124-4126.

[32] I. G. Hill, D. Milliron, J. Schwartz and A. Kahn, *Applied Surface Science* **2000**, *166*, 354-362.

[33] G. Kresse and J. Hafner, *Physical Review B* **1993**, *47*, 558-561.

[34] G. Kresse and J. Hafner, *Physical Review B* **1994**, *49*, 14251-14269.

[35] G. Kresse and J. Furthmuller, *Computational Materials Science* **1996**, *6*, 15-50.

[36] G. Kresse and J. Furthmuller, *Physical Review B* **1996**, *54*, 11169-11186.

[37] M. Born and R. Oppenheimer, *Annals of Physics* **1927**, *84*, 457.

[38] D. R. Hartree, *Proceedings Of The Cambridge Philological Society* **1928**, *24*, 111-133.

[39] P. Hohenberg and W. Kohn, *Physical Review B* **1964**, *136*, B864-&.

[40] W. Kohn and L. J. Sham, *Physical Review* **1965**, *140*, 1133-&.

[41] J. P. Perdew, K. Burke and M. Ernzerhof, *Physical Review Letters* **1996**, *77*, 3865-3868.

[42] J. P. Perdew and W. Yue, *Physical Review B* **1986**, *33*, 8800-8802.

[43] J. P. Perdew, J. A. Chevary, S. H. Vosko, K. A. Jackson, M. R. Pederson, D. J. Singh and C. Fiolhais, *Physical Review B* **1992**, *46*, 6671-6687.

[44] D. Vanderbilt, *Physical Review B* **1990**, *41*, 7892-7895.

[45] G. Kresse and J. Hafner, *Journal Of Physics-Condensed Matter* **1994**, *6*, 8245-8257.

[46] G. Kresse and D. Joubert, *Physical Review B* **1999**, *59*, 1758-1775.

[47] P. E. Blochl, *Physical Review B* **1994**, *50*, 17953-17979.

[48] P. E. Blochl, O. Jepsen and O. K. Andersen, *Physical Review B* **1994**, *49*, 16223-16233.

[49] C. **Kittle**, *Introduction to Solid State Physics, Wiley, New York,* **1996**.

[50] M. Methfessel and A. T. Paxton, *Physical Review B* **1989**, *40*, 3616-3621.

[51] P. Pulay, *Chemical Physics Letters* **1980**, *73*, 393-398.

[52] G. Mills, H. Jonsson and G. K. Schenter, *Surface Science* **1995**, *324*, 305-337.

[53] H. Jonsson, G. Mills and K. W. Jacobsen, *World Scientific* **1998**.

[54] J. Neugebauer and M. Scheffler, *Physical Review B* **1992**, *46*, 16067-16080.

[55] G. Kirczenow, P. G. Piva and R. A. Wolkow, *Physical Review B* **2005**, *72*.

[56] Y. Pei and J. Ma, *Langmuir* **2006**, *22*, 3040-3048.

[57] J. K. Kang and C. B. Musgrave, *Journal Of Chemical Physics* **2002**, *116*, 9907-9913.

[58] J. H. Cho, D. H. Oh and L. Kleinman, *Physical Review B* **2002**, *65*.

[59] N. Takeuchi and A. Selloni, *Journal Of Physical Chemistry B* **2005**, *109*, 11967-11972.

[60] J. L. Pitters, I. Dogel, G. A. DiLabio and R. A. Wolkow, *The Journal of Physical Chemistry. B, Condensed matter, materials, surfaces, interfaces & biophysical* **2006**, *110*, 2159.

[61] X. Tong, G. A. DiLabio and R. A. Wolkow, *Nano Letters* **2004**, *4*, 979-983.

[62] R. Wolkow and R. Luck, *Not puplished*.

[63] A. I. Shkrebtii, R. Defelice, C. M. Bertoni and R. Delsole, *Physical Review B* **1995**, *51*, 11201-11204.

[64] C. Sgiarovello, N. Binggeli and A. Baldereschi, *Physical Review B* **2001**, *64*.

[65] N. Takagi, N. Minami and M. Nishijima, *Physical Review B* **1992**, *45*, 13524-13530.

[66] A. E. Souzis, M. Seidl, W. E. Carr and H. Huang, *Journal Of Vacuum Science & Technology A-Vacuum Surfaces And Films* **1989**, *7*, 720-723.

[67] D. S. Vlachos and C. A. Papageorgopoulos, *Journal Of Physics-Condensed Matter* **1996**, *8*, 8799-8814.

[68] A. Michaelides, P. Hu, M. H. Lee, A. Alavi and D. A. King, *Physical Review Letters* **2003**, *90*.

[69] A. Natan, L. Kronik and Y. Shapira, *Applied Surface Science* **2006**, *252*, 7608-7613.

[70] A. Natan, Y. Zidon, Y. Shapira and L. Kronik, *Physical Review B* **2006**, *73*.

[71] E. P.J. Linstrom and W.G. Mallard, NIST Chemistry WebBook, NIST Standard Reference Database Number 69, June **2005**, National Institute of Standards and Technology, Gaithersburg MD, 20899 (http://webbook.nist.gov).

[72] D. A. Pratt, G. A. Dilabio, P. Mulder and K. U. Ingold, *Accounts Of Chemical Research* **2004**, *37*, 334-340.

[73] G. A. DiLabio, D. A. Pratt and J. S. Wright, *Journal Of Organic Chemistry* **2000**, *65*, 2195-2203.

[74] C. G. Broyden, *Mathematics Of Computation* **1965**, *19*, 557-593.

[75] D. D. Johnson, *Physical Review B* **1988**, *38*, 12807-12813.

[76] H. J. Monkhorst and J. D. Pack, *Physical Review B* **1976**, *13*, 5188-5192.

Appendix A

Vienna *Ab initio* Simulation Package (VASP)

VASP uses plane waves (PW) as basis functions to solve the Kohn and Sham equations. Because of the basis functions, the wave functions consist of Fourier series, which goes on to infinity. Below are the procedures and the implementation of VASP for solving the wave equations.

The electron wave function is expanded in a Fourier series as

$$\Psi = \sum_{n,\vec{k}} \Psi_{n,\vec{k}}(\vec{r}) e^{i\vec{k}\bullet\vec{r}} \qquad \text{(A.1)}$$

When electron state in a solid is considered in the periodic system, then we can make use of a very useful theorem to simplify the problem, the Bloch theorem. Bloch's theorem says that any wave function of a periodic system is the product of a cell-periodic part and a phase factor (a wave like part). This preserves the translational symmetry of the density. The phase factor takes the form of a plane wave, whose wave vector is a linear combination of reciprocal lattice vectors. Hence, the wave function consists of the product of a plane wave and a periodic function $u_{n,\vec{k}}(\vec{r})$, which has the same periodicity as the potential

$$\Psi_{n,\vec{k}}(\vec{r}) = u_{n,\vec{k}}(\vec{r}) e^{i\vec{k}\bullet\vec{r}} \qquad \text{(A.2)}$$

The plane wave vector $\vec{k}$ is unique only up to a reciprocal lattice vector, so one only needs to consider the wave vectors inside the Brillouin zone. The Brillouin zone is the smallest primitive cell in the k-space. For a given wave vector and potential, there are a number of solutions, indexed by n, to the Schrödinger's equation for a Bloch electron. These solutions are separated in energy by a finite spacing. This space is called band gap. The band structure is the collection of energy eigenstates within the first Brillouin zone. All the properties of electrons in a

periodic potential can be calculated from this band structure. All other information of a system can be determined within the first primitive cell within the independent electron approximation.

In the Bloch's theorem, it can be shown that the wave function of a particle in a periodic potential must have the form as in Eq. A.1 and A.2, translational operators (lattice vector) commute with the Hamiltonian. The Bloch theorem implies that the single electron wave functions is expressed as

$$\Psi_{n,\vec{k}}(\vec{r}+\vec{\tau}) = \Psi_{n,\vec{k}}(\vec{r})e^{i\vec{k}\bullet\vec{\tau}} \tag{A.3}$$

where $\vec{\tau}$ is any translational vector leaving the Hamiltonian invariant. The wave function determines other physical quantities, for example, the charge density is determined by integrating over the entire Brillounin zone and summing over the filled bands

$$n(\vec{r}) = \sum_n^{\infty} \int d^3\vec{k} f_{n,\vec{k}} \left|\Psi_{n,\vec{k}}(\vec{r})\right|^2 \tag{A.4}$$

Here the vector k runs over the set of **k**-points and n labels the occupied states, and the integral over the Brillouin zone is replaced by a sum over the discrete k-point set.

The charge density is cell periodic (obeys Bloch's theorem) and $f_{n,\vec{k}}$ is the Fermi-weight is given by

$$f_{n,\vec{k}} = \frac{1}{\exp(\beta(\varepsilon_{n,\vec{k}} - \varepsilon_{Fermi}))+1} \tag{A.5}$$

where $\beta = 1/K_B T$, K_B is the Boltzmann constant and T is the temperature .
Finally the Kohn and Sham DFT equations are written as

$$\left[-\frac{\hbar^2}{2m}\nabla^2 + V_{eff}(\vec{r},[n_e(\vec{r}')])\right]\Psi_{n,\vec{k}}(\vec{r}) = \varepsilon_{n,\vec{k}}\Psi_{n,\vec{k}}(\vec{r}) \tag{A.6}$$

where

$$V_{eff}(\vec{r},[n_e(\vec{r})]) = e^2 \int \frac{n_e(\vec{r}') + n_{ion}(\vec{r})}{|\vec{r} - \vec{r}'|} d^3\vec{r}' + V_{xc}([n_e(\vec{r})]) \qquad (A.7)$$

$n_{ion}(\vec{r})$ is the ionic charge distribution

$$\left[-\frac{\hbar^2}{2m}\nabla^2 + V_{eff}(\vec{r},[n_e(\vec{r}')]) \right] \Psi_{n,\vec{k}}(\vec{r}) = \varepsilon_{n,\vec{k}} \Psi_{n,\vec{k}}(\vec{r}) \qquad (A.8)$$

All periodic functions are now written as a sum of plane waves

$$u_{n,\vec{k}}(\vec{r}) = \frac{1}{\sqrt{V_{cell}}} \sum_{\vec{G}} C_{\vec{G},n,\vec{k}} e^{i\vec{G}\bullet\vec{r}} \qquad (A.9)$$

$$\Psi_{n,\vec{k}}(\vec{r}) = \frac{1}{\sqrt{V_{cell}}} \sum_{\vec{G}} C_{\vec{G},n,\vec{k}} e^{i(\vec{G}+\vec{k})\bullet\vec{r}} \qquad (A.10)$$

The electron density and the potential is expressed as

$$n(\vec{r}) = \sum_{\vec{G}} n_{\vec{G}} e^{i\vec{G}\bullet\vec{r}} \qquad (A.11)$$

$$V(\vec{r}) = \sum_{\vec{G}} V_{\vec{G}} e^{i\vec{G}\bullet\vec{r}} \qquad (A.12)$$

Inserting these expressions into the Kohn and Sham DFT equation (A.6), one obtains

$$\sum_{\vec{G}} \left\{ -\frac{\hbar^2}{2m} \left| \vec{G} + \vec{K} \right|^2 - \varepsilon_{n,\vec{k}} \right\} C_{\vec{G},n,\vec{k}} e^{i(\vec{G}+\vec{k})\bullet\vec{r}} + \sum_{\vec{G},\vec{G}'} V_{\vec{G}'} C_{\vec{G},n,\vec{k}} e^{i(\vec{G}'+\vec{G}+\vec{k})\bullet\vec{r}} = 0 \qquad (A.13)$$

If we then multiply the above set of equations by an orthogonal function $e^{-i(\vec{G}''+\vec{k})\bullet\vec{r}}$ and integrated over the volume of the crystal, creates Kronecker delta functions as

$$\sum_{\vec{G}}\left\{-\frac{\hbar^2}{2m}\left|\vec{G}+\vec{K}\right|^2-\varepsilon_{n,\vec{k}}\right\}C_{\vec{G},n,\vec{k}}\delta_{\vec{G},\vec{G}''}+\sum_{\vec{G},\vec{G}'}V_{\vec{G}'}C_{\vec{G},n,\vec{k}}\delta_{\vec{G}',\vec{G}''-\vec{G}}=0 \qquad \text{(A.14)}$$

In the above equation, one summation in each term can be eliminated. For example, in the first term, $\vec{G}$ and $\vec{G}''$ must be equal in order to have non-zero term. Thus the summation over $\vec{G}$ includes only one non-zero term. Likewise, a summation can be eliminated from each of the other two terms.

$$\left\{-\frac{\hbar^2}{2m}\left|\vec{G}+\vec{K}\right|^2-\varepsilon_{n,\vec{k}}\right\}C_{\vec{G},n,\vec{k}}+\sum_{\vec{G}'}V_{\vec{G}-\vec{G}'}C_{\vec{G},n,\vec{k}}=0 \qquad \text{(A.15)}$$

The equation can be cast as an eigenvalue equation with the following matrix form.

$$\left\{-\frac{\hbar^2}{2m}\left|\vec{G}+\vec{K}\right|^2+\sum_{\vec{G}'}V_{\vec{G}-\vec{G}'}-\varepsilon_{n,\vec{k}}\right\}C_{\vec{G},n,\vec{k}}=0 \quad \Rightarrow \left\{H-\varepsilon_{n,\vec{k}}\right\}C_{\vec{G},n,\vec{k}}=0 \text{(A.16)}$$

where H represents the Hamiltonian matrix element, which includes the sum of the first two terms from the left side of the equation.

If the Fourier series were not truncated in the expansion of the PW at each k-point, then the matrix would be infinite in size and difficult to solve in any calculation, so one has to cut the series somewhere. However, in simulation more PW is important, the more accurately it represents the actual wave function but more expensive in simulation. A cutoff energy is set such that all PW with a higher energy are excluded

$$-\frac{\hbar^2}{2m}\left|\vec{G}+\vec{K}\right|^2 < E_{cutoff} \qquad \text{(A.17)}$$

From Eq. A.17, the wave function is then defined as a linear sum of plane waves, each with a unique energy. Assuming all expansion coefficients are non-zero , the determinant (Eq. A.16) is calculated as

$$\det\left(H-\varepsilon_{n,\vec{k}}\right)=0 \tag{A.18}$$

$$\det\begin{bmatrix} H_{11}-\varepsilon_{n,\vec{k}} & H_{12} & \dots & H_{1N} \\ H_{21} & H_{22}-\varepsilon_{n,\vec{k}} & \dots & H_{2N} \\ \vdots & \vdots & & \vdots \\ H_{N1} & H_{N2} & \dots & H_{NN}-\varepsilon_{n,\vec{k}} \end{bmatrix}=0 \tag{A.19}$$

For a basis set of N functions, there is a maximum of N different real eigenvalues. There might be more than N eigenvalues, but only N of them will be unique and real. These unique eigenvalues reside along the diagonal of the Hamiltonian matrix where all off-diagonal values are zero. Such matrix is called diagonalized matrix.

$$\begin{bmatrix} H_{11} & H_{12} & \dots & H_{1N} \\ H_{21} & H_{22} & \dots & H_{2N} \\ \vdots & \vdots & & \vdots \\ H_{N1} & H_{N2} & \dots & H_{NN} \end{bmatrix}\begin{bmatrix} a_1\Psi_1 \\ a_2\Psi_2 \\ \vdots \\ a_N\Psi_N \end{bmatrix}=\varepsilon_i\begin{bmatrix} a_1\Psi_1 \\ a_2\Psi_2 \\ \vdots \\ a_N\Psi_N \end{bmatrix} \tag{A.20}$$

$$\int\Psi_i^*\hat{H}\Psi d^3\vec{r}=<\Psi_i|\hat{H}|\Psi_i>=\varepsilon_i \tag{A.21}$$

A wave function multiplied by its complex conjugate equals its amplitude or probability density, so the integral above yields the eigenvalue ε_i^{th} with probability of occurrence a_i. These expansion coefficients equate to the occupation numbers for each orbital. Once the eigenvalues are obtained, the total energy and density are calculated, thereby ending one self-consistent loop. Each base function and its corresponding occupation number and energy eigenvalue at the end of each loop is used as input into the subsequent loop.

Many terms in the Hamiltonian matrix are approximately or exactly zero in many types of calculations and various algorithms have been developed that take

advantage of this fact to speed up matrix diagonalization. For VASP specifically, ground state energies and charge densities are calculated using a Pulay-like mixing scheme [51, 74, 75] and one of three minimization algorithms: conjugate gradient (CG), Davidson blocked iteration (DAV), or residuum-minimization method by direct inversion in the iterative subspace (RMM-DIIS).

A.1. K-point Sampling

Energies in the Brillouin Zone (BZ) in the reciprocal space are sampled using a 3-D grid of **k**-points $\{\vec{k} : \vec{k} = (k_x, k_y, k_z)\}$. The larger the system in real space, the smaller it is in reciprocal space; and so the fewer the **k**-points needed to precisely (but not necessarily accurate) calculate the energy. The occupied states at each **k**-point contribute to the electronic potential of the system. It is based on the assumption that the electronic wave functions at **k**-points that are very close together will almost be identical and can be sampled by discrete set of points. This approximation allows the electronic potential/charge to be calculated at a finite number of **k**-points and hence determine the total ground state energy of the solid.

In most simulations, the defined **k**-point grid is reduced via symmetry operations to a set of irreducible **k**-points called the irreducible Brillouin Zone (IBZ). Each point in the IBZ is defined by its unique position in reciprocal space, and its weight. No two points in the IBZ have the same position, but multiple points can have the same weight. The IBZ is the set of unique points needed to precisely sample a given crystal structure. Any additional point will be a symmetric copy of an existing point in the IBZ and so is not needed. The integration is done in practice by summing over a relatively small number of **k**-points in the irreducible segment of the Brillouin zone and then using the lattice symmetry to extend this result to the rest of the zone.

VASP offers two grid geometries, which are specified in the K-POINTS file: Monkhorst-Pack (MP) [50, 76] and Gamma Centered (GC). In the Monkhorst-Pack [21] representation, equally spaced mesh is used in the Brillouin-zone.

A **k**-vector in the reciprocal space is give by

$$\vec{K}_{prs} = u_p \vec{b}_1 + u_r \vec{b}_2 + u_s \vec{b}_3 \qquad \text{(A.22)}$$

$$u_r = \frac{2r - q_r - 1}{2q_r} \qquad r = 1, 2, \ldots, q_r \qquad \text{(A.23)}$$

where $\vec{b}_i$ is the reciprocal lattice-vectors and q_r determines number of **k**-points in r-direction.

The integral, I, for many properties like density of states, charge density, matrix elements, response function, over the Brillouin zone is carried out as

$$I(\varepsilon) = \frac{1}{V_{BZ}} \int_{BZ} F(\varepsilon)\delta(\varepsilon_{n\vec{k}} - \varepsilon)d\vec{k} \qquad \text{(A.24)}$$

To evaluate integrals computationally, one has to convert the integral to discreet point weighted over special **k**-points

$$\frac{1}{V_{BZ}} \int_{BZ} \Rightarrow \sum_{\vec{k}} w_{\vec{k}_i} \qquad \text{(A.25)}$$

The Fourier transformation of any function is expressed as

$$f(\vec{r}) = \frac{V}{(2\pi)^3} \int_{BZ} F(k)dk = \sum_i w_{k_i} F(k_i) \qquad \text{(A.26)}$$

where $F(\vec{k})$ is the Fourier transform of $f(\vec{r})$, V is the cell volume and the w_{k_i}'s are weighting factors.

The **k**-points are distributed uniformly through space. A further computational saving may be made by utilizing the point group symmetry of the lattice. This allows one to write the sums as

$$f(\vec{r}) = \sum_{i=1}^{k_{irr}} w_{k_i} F(k_i) \qquad \text{(A.27)}$$

where k_{irr} is the symmetry-dependent number of points in the irreducible wedge of the Brillouin zone.

Appendix B

Testing the simulation parameters

The bulk properties of silicon and the optimal values of each parameter used in the calculations were performed so that these parameters can be used for surface calculations. The **k**-point, plane wave cutoff energy convergences were tested. The lattice constant of silicon is obtained from the energy versus volume calculation.

The most common form of silicon element has a bulk structure of diamond in which every atom of silicon is covalently bonded by for silicon atom. The smallest unit cell for making this bulk structure has Face centered structure consisting of two silicon atoms.

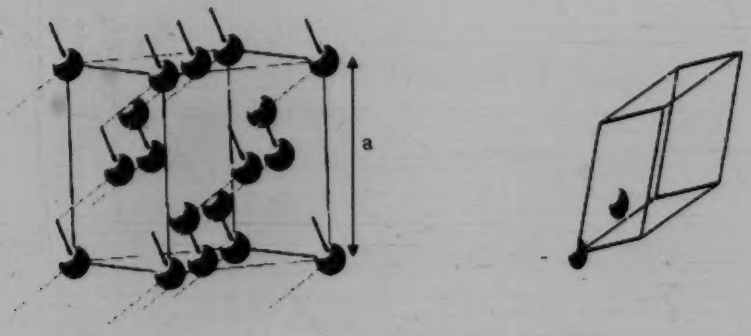

(a) (b)

Figure B.1 The diamond structure of silicon (a) and its primitive cell (b)

B.1. K-point convergence

K-point convergence is done to determine the geometry, and the minimal number of grid points needed to calculate the energy of a system. The **k**-point setting has the form (X Y Z), where the three coordinates are the number of points along the x, y, and z directions in the BZ. Here below is the ground state energy of silicon bulk

obtained at different **k**-points. The result obtained helps to determine which **k**-point set to use during the next surface simulations.

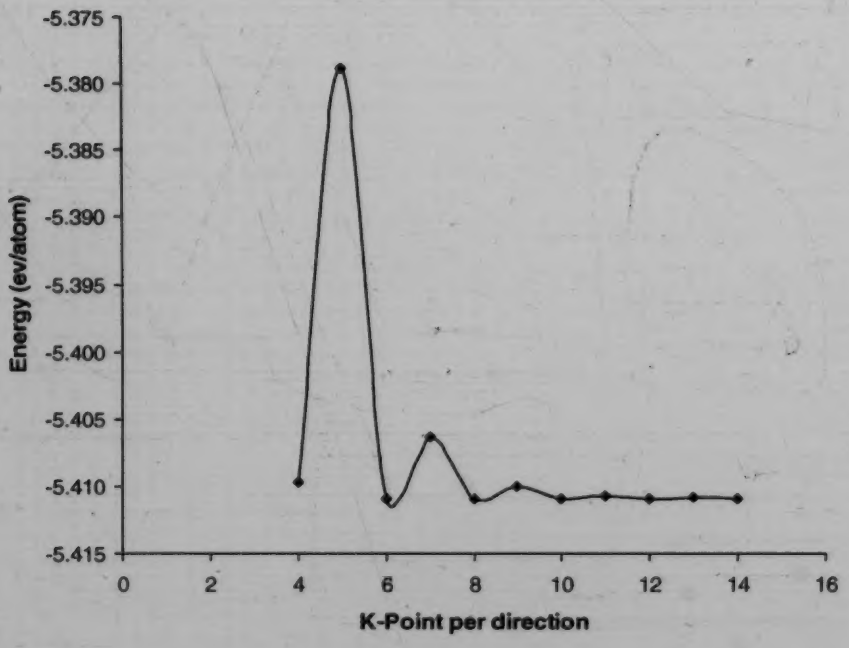

Figure B.2 Convergence of Si cohesive energy versus number of **k**-points per direction.

Table B.1 Energy change per atom calculated at different **k**-point meshes and irreducible k-points.

K-POINTS grid size (no units)	Number of irreducible k-points	Energy per atom (eV/atom)	Energy change (meV/atom)
4 4 4	10	-5.40966	0.000000
5 5 5	10	-5.37882	30.845000
6 6 6	28	-5.41090	-32.086500
7 7 7	20	-5.40632	4.580500
8 8 8	60	-5.41093	-4.609000
9 9 9	35	-5.40997	0.957000
1010 10	110	-5.41093	-0.954500
11 11 11	56	-5.41075	0.175000
12 12 12	182	-5.41093	-0.172500
13 13 13	84	-5.41087	0.052000
14 14 14	280	-5.41091	-0.033000

As we can see from Table B.1, the larger **k**-point grids does not always give a dense number of irreducible k-points reside in the Brillounin zone. In principle, it is always a good idea to use many **k**-points whenever possible. In most simulations, however, the defined **k**-point grid is reduced via symmetry to a set of irreducible **k**-points. For instance, 9x9x9 mesh has less irreducible k-points (35) than 10x10x10 mesh (110) requires less computational time but the cohesive energy is similar within a few m eV differences. The 10x10x10 and 11x11x11 meshes give the same energy; the difference is 0.95 meV/atom but 10x10x10 mesh has more irreducible k-points than 11x11x11. Compared to the 12x12x12 mesh, the 11x11x11 mesh gives the energy less by very few 0.18 meV/atom (see Table B.1). Nonetheless, the 11x11x11 mesh needs small irreducible k-points as compared to 10x10x10 and 12x12x12 meshes. For the final bulk silicon crystal calculations, the 11x11x11 k-point sampling was used. This k-point is used for the reported lattice constant of

silicon. However, for surface calculations to evenly divide surface in the reciprocal space accordingly, the choice of 10x10x10 mesh is more convenient to use.

B.2. Cutoff energy convergence

When using any other plane wave method, the terms of the series that describing the wave function can be expressed in terms of their energy has to converge. So, one has to make sure that the cutoff energy should be large enough such that the total energy is converged.

Table B.2 Convergence of cohesive energy change per atom calculated at different cutoff energies.

Cutoff E energy (eV)	Energy (eV/atom)	Energy change (meV/atom)
184.009	-5.39173	0.000
204.009	-5.40045	-8.728
224.009	-5.40622	-5.768
244.009	-5.41063	-4.407
264.009	-5.41467	-4.046
284.009	-5.41748	-2.806
304.009	-5.41944	-1.958
324.009	-5.42047	-1.027
344.009	-5.42111	-0.645
364.009	-5.42163	-0.517
384.009	-5.42200	-0.377
404.009	-5.42222	-0.218
424.009	-5.42230	-0.079
444.009	-5.42232	-0.018
464.009	-5.42232	0.000
484.009	-5.42230	0.018
504.009	-5.42230	0.002

In Table B.2, we see that the cutoff energy of 384 eV is enough to calculate the bulk properties of silicon crystal. At this energy, the ground state energy is converged within 0.5 meV/atom. However, when silicon is combined with other elements a careful convergence of the cutoff energy is considered.

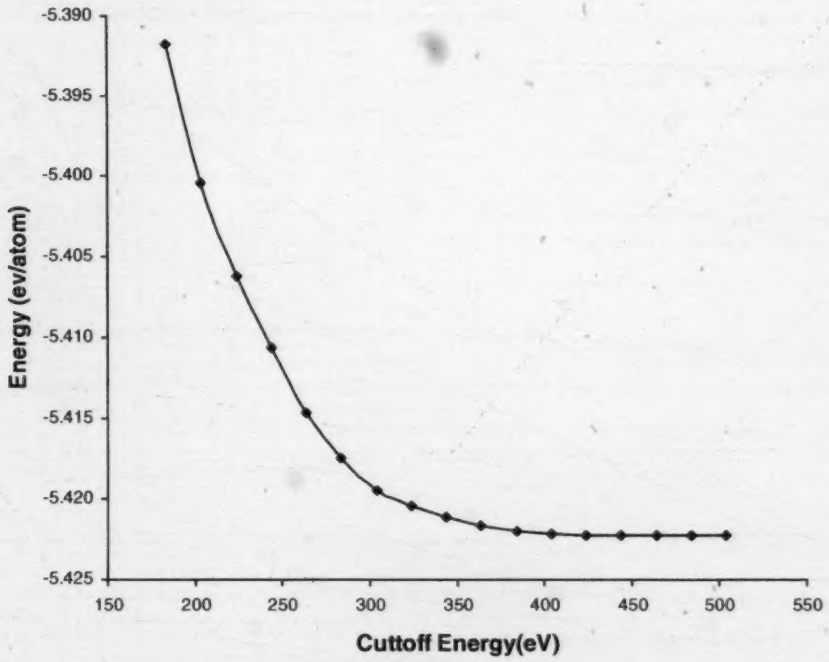

Figure B.3 Convergence of Si cohesive energy versus cutoff energy.

Once the convergence of the **k**-points and the cutoff energy are determined, the energy versus volume test is used to calculate the cohesive energy (E_0), lattice constants (a_o), and bulk modulus (B_o) at 0 K. On the other hand a test of PP must be done so that the PP that gives values of these parameters closest to actual values is then usually used for other calculations. The E_0 of an elemental solid is often referred to as binding energy. This is the energy/atom needed to remove an atom from the crystal solid and place it infinitely far away.

The lattice constant of Si atom was obtained from bulk calculations by fitting to an equation of state using Murnaghan equation. The Murnaghan equation is given by

$$E(V)=\frac{B_o V}{B_o'(B_o'-1)}\left[B_o'(1-\frac{V_o}{V})+\left(\frac{V_o}{V}\right)^{B_o'}-1\right]+E_o(V_o) \qquad \text{(B.1)}$$

B_o is isothermal bulk modulus (eV/Å^3), Eo is cohesive energy (eV/atom), Bo' is pressure derivative of the isothermal bulk modulus and Vo is equilibrium volume (Å^3), all at zero pressure. E (V) is cell energy from the electronic relaxation of cell with volume V, and V is cell volume (Å^3). The Murnaghan equation of state assumes that B_o can be expressed as a Taylor series of the pressure.

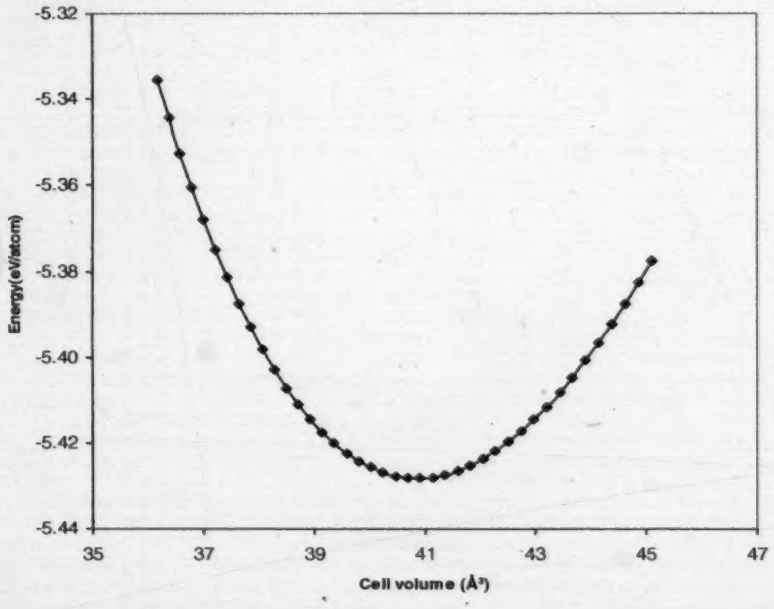

Figure B.4 Cohesive energy/atom of silicon bulk versus the volume of the cell. The minimum of the plot gives the optimum lattice constant.

In Fig. B.4, the fit gives a lattice constant of 5.459 Å close to the experimental value of 5.43 Å. In this fitting the isothermal bulk modulus (eV/Å^3) at zero pressure is

found 889.64 eV/Å^3, where the experimental value is about 999.9 eV/Å^3. The fit also gives pressure derivative of the isothermal bulk modulus at zero pressure close to 4.262.

The pseudopotential for silicon was tested with simple bulk calculations. Among the PP given by VASP, the PAW PP of the PBE functional form gives the lattice constant closer to the experimental value than the other. In so doing, all the surface calculations are done through the PAW PP using PBE functional. All silicon based surface calculations in this thesis were performed using the calculated equilibrium lattices constant. It is important that careful convergence of the cutoff energy, k-points sampling and choice of PP should be performed when silicon is combined with other elements.

The energy level of electrons in a periodic solid can be classified into energy bands (see Fig. B.5). Other physical quantities such as the band gap, density of states (DOS), Fermi energy and total energy can be obtained from the band structure.

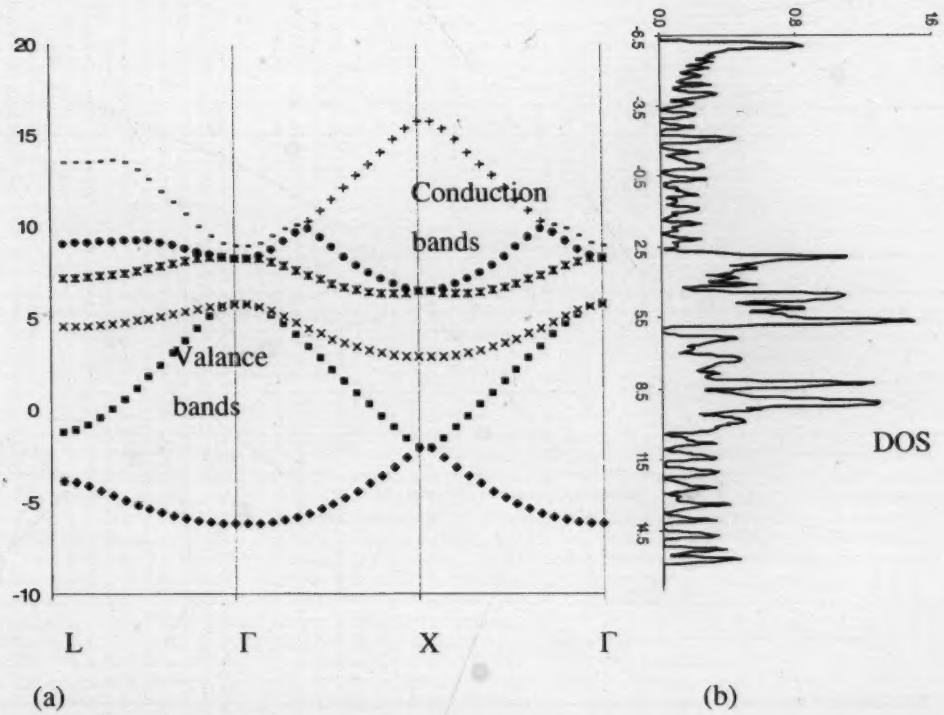

Figure B.5 (a) Band structure of silicon along a high symmetry line obtained by GGA-PBE functional at the equilibrium lattice constant. (b) The DOS of silicon bulk crystal.

The band structure diagram contains valuable information. For instance, the band gab, which is the difference between the highest occupied valance band and the lowest unoccupied conduction band, can be obtained. The band gap determines the semiconductor's conductivity.

Appendix C

FLOWCHART

Below is a flowchart showing what VASP does in performing a Single point energy calculation. This flowchart is applicable to the time-independent DFT code that uses the plane wave expansion, pseudopotentials, and the Born–Oppenheimer approximation and hence VASP uses the following flowchart

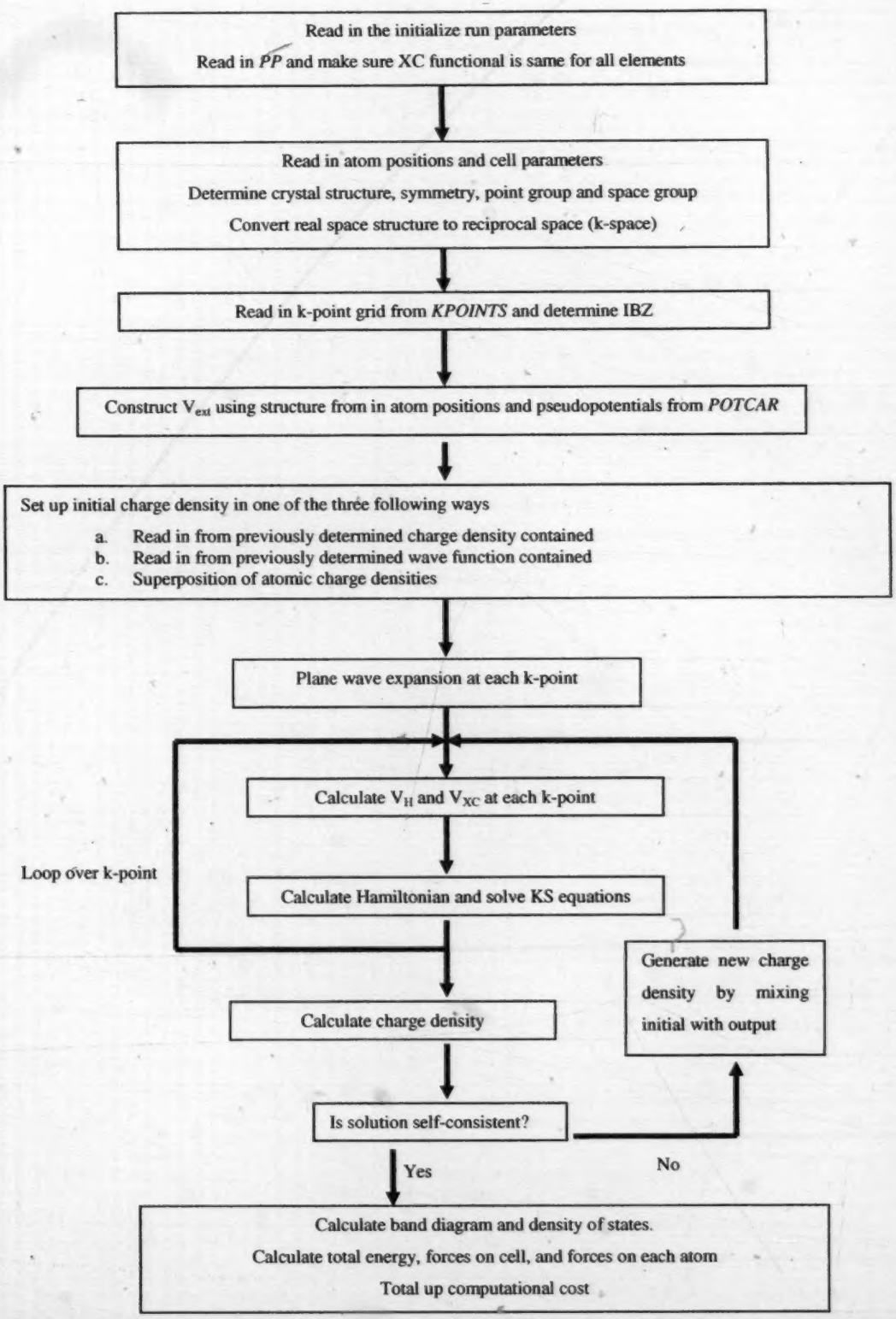
Read in the initialize run parameters
Read in PP and make sure XC functional is same for all elements
Read in atom positions and cell parameters
Determine crystal structure, symmetry, point group and space group
Convert real space structure to reciprocal space (k-space)
Read in k-point grid from KPOINTS and determine IBZ
Construct V_{ext} using structure from in atom positions and pseudopotentials from POTCAR
Set up initial charge density in one of the three following ways
a. Read in from previously determined charge density contained
b. Read in from previously determined wave function contained
c. Superposition of atomic charge densities
Plane wave expansion at each k-point
Loop over k-point
Calculate V_H and V_{XC} at each k-point
Calculate Hamiltonian and solve KS equations
Generate new charge density by mixing initial with output
Calculate charge density
Is solution self-consistent?
No
Yes
Calculate band diagram and density of states.
Calculate total energy, forces on cell, and forces on each atom
Total up computational cost